PROCEEDINGS A

royalsocietypublishing.org/journal/rspa

Research

Cite this article: Bruna M, Chapman SJ, Schmidtchen M. 2023 Derivation of a macroscopic model for Brownian hard needles. *Proc. R. Soc. A* **479**: 20230076. https://doi.org/10.1098/rspa.2023.0076

Received: 1 February 2023
Accepted: 16 May 2023

Subject Areas:
applied mathematics

Keywords:
many-particle systems, anisotropic particles, excluded-volume interactions, phase transitions, coarse-graining

Author for correspondence:
Maria Bruna
e-mail: bruna@maths.cam.ac.uk

Electronic supplementary material is available online at https://doi.org/10.6084/m9.figshare.c.6673715.

THE ROYAL SOCIETY PUBLISHING

Derivation of a macroscopic model for Brownian hard needles

Maria Bruna[1], Stephen J. Chapman[2] and Markus Schmidtchen[3]

[1]Department of Applied Mathematics and Theoretical Physics, University of Cambridge, Wilberforce Road, Cambridge CB3 0WA, UK
[2]Mathematical Institute, University of Oxford, Andrew Wiles Building, Radcliffe Observatory Quarter, Woodstock Road, Oxford OX2 6GG, UK
[3]Institute of Scientific Computing, Technische Universität Dresden, Zellescher Weg 12-14, 01069 Dresden, Germany

MB, 0000-0001-7829-5652; SJC, 0000-0003-3347-6024; MS, 0000-0001-9662-3111

We study the role of anisotropic steric interactions in a system of hard Brownian needles in two dimensions. Despite having no volume, non-overlapping needles exclude a volume in configuration space that influences the macroscopic evolution of the system. Starting from the stochastic particle system, we use the method of matched asymptotic expansions and conformal mapping to systematically derive a nonlinear non-local partial differential equation for the evolution of the population density in position and orientation. We consider the regime of high rotational diffusion, resulting in an equation for the spatial density that allows us to compare the effective excluded volume of a hard-needle system with that of a hard-sphere system. We further consider spatially homogeneous solutions and find an isotropic to nematic transition as density increases, consistent with Onsager's theory.

1. Introduction

Systems of interacting particles are ubiquitous in nature. Examples include biomolecules (e.g. proteins), polymers (e.g. DNA), cells (e.g. bacteria) and all the way to multicellular organisms (animals). Interactions between

organisms may be attractive (keeping a herd cohesive), aligning (keeping animals moving in the same direction) or repulsive (keeping particles a safe distance apart) [1]. Short-ranged repulsive interactions with singular or hard-core potentials are used to model steric or excluded-volume interactions [2].

Anisotropy plays a crucial role in self-organization. For example, the helical form of the DNA strand is due to highly anisotropic interactions between DNA bases [3]. The molecular shape of liquid crystals leads to their remarkable properties [4]. Self-propulsion in active matter systems can lead to motility-induced phase separation [5], where the uniform suspension becomes unstable and dense clusters of almost stationary particles emerge [5]. Alignment interactions have been shown to explain the emergence of flocking and milling [6].

Tools to study the rich collective properties of such systems range from simulations at the microscopic level (e.g. molecular dynamics or Monte Carlo simulations) to the study of macroscopic models for statistical quantities, often involving partial differential equations (PDEs). While microscopic models provide a detailed system description, simulating them can become computationally prohibitive. This is due to the large number of particles and the complexity of interactions often involved, mainly if one is after statistical properties (which require averaging over multiple simulations). Macroscopic models operate at the statistical level and can often provide the insight lacking in their microscopic counterparts.

Anisotropy in particle systems comes in many forms. Models can be classified into either first- or second-order models and either soft- or hard-core interactions. In second-order models (which track particles' positions and velocities), particles may interact differently depending on their relative velocities. Examples with weak interactions include the Cucker–Smale model [7], and the Vicsek model [8], which include alignment interactions in velocities. One may also add a cone of vision such that an individual only aligns velocity with neighbours within the cone [6]. The Cucker–Smale and Vicsek models, and their many variants, have been the starting point in multiple works concerned with deriving kinetic PDE models starting from such microscopic dynamics. It is common to consider a weak or mean-field scaling $1/N$ of the interactions (where N is the number of particles), leading to non-local and nonlinear kinetic PDE in the limit [9–13]. The focus in most kinetic models is on how the interaction rule depends on relative positions and velocities, not particles' shapes. An exception is the recent works [14,15], where they consider a system of kinetic hard needles that align upon collision. Instead of a mean-field scaling, they consider the Boltzmann–Grad limit of infrequent but strong interactions and invoke propagation of chaos to derive a closed kinetic equation.

First-order models for anisotropic particles often consider the particle position and orientation and assume diffusive behaviour in both. For isotropic particles, microscopic models are well established (the hard-sphere, the Lennard–Jones, the Coulomb potential, etc.), and current efforts primarily focus on deriving macroscopic models from them. By contrast, anisotropic particles are much harder to model, even at the microscopic scale. There is a trade-off between the complexity of the particles' shape, on the one hand, and the model's analytic tractability, on the other hand. Interactions may be soft or hard depending on the application, either may be seen as the 'true dynamics'. For example, while soft interactions may be more appropriate for molecules, hard steric interactions may be more fitting for cells, bacteria and animals.

The most well-known soft anisotropic potential is the Gay–Berne potential [16]. It builds on the work of Berne & Pechukas [17], which proposed to represent particles as a union of Gaussian potentials and their interaction as the overlap integral of their Gaussians. The Gay–Berne potential combines this anisotropic overlap model with the Lennard–Jones potential (a 12-6 attractive-repulsive potential). The multi-phase-field approach [18,19] is at the other end of the complexity-tractability trade-off. Here, each particle is not characterized by its centre of mass and orientation but by a phase field variable, $\phi_i(x,t) \in [0,1]$, such that $\phi_i(x,t) \approx 1$ if location x is occupied by the particle i at time t and, conversely, $\phi(x,t) \approx 0$ if the ith particle does not occupy location x at time t. Due to the diffusive interface between the two states (occupied and unoccupied), repulsive interactions are incorporated in a fashion similar to that of Berne and Pechukas: the overlap integral between two particles (now represented by phase-field

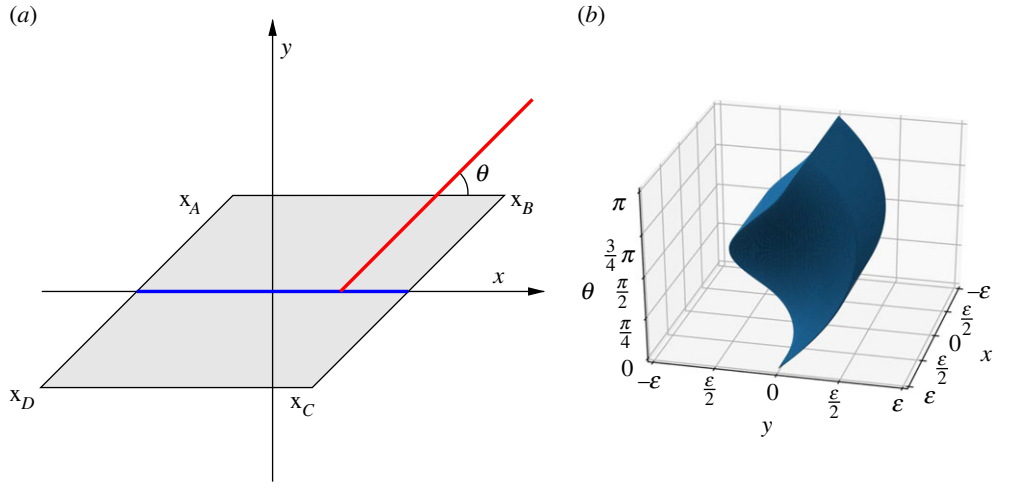

Figure 1. (*a*) Excluded volume of a horizontal hard needle (blue) with centre at the origin. The centre of a second needle (red) with orientation θ cannot be placed inside the excluded region (shaded grey area) as it would lead to an overlap. (*b*) Excluded volume in phase space. The vertical axis denotes the relative angle between two needles.

variables rather than Gaussian) is computed, and the evolution is such that it minimizes the area of overlap.

The aforementioned models have in common that the space taken up by particles is not precisely localized, in contrast to hard-core models. Hard-core ellipsoids and rods are the natural generalizations of hard spheres to model anisotropy. A hard-core particle induces an excluded region (where no other particle can enter). In his seminal paper [20], Onsager finds expressions for the excluded volume of various particle shapes such as ellipses, discs and rods. The most striking example in his treatise is a hard needle of length ϵ in two dimensions, which has zero volume but excludes a volume in configuration space of $\epsilon^2|\sin(\theta)|$ to another needle with relative orientation θ (figure 1). The problem of interacting needles in three dimensions is fundamentally different since needles exclude zero volume in configuration space in addition to having no volume. Rods with a core-shell structure have also been used in microscopic models of self-assembly [21] and morphogenesis in bacterial colonies [22]. Interesting mathematical problems arise from considering even just one anisotropic hard-core particle. For example, in the study by Holcman & Schuss [23], they study the mean turnaround time of a Brownian needle in a narrow planar strip as a simplified model for mRNA or stiff DNA fragments under extreme confinement. In the study by Chen & Thiffeault [24], they consider an anisotropic Brownian microswimmer in a channel and show that no-flux boundary conditions with the flat channel walls lead to non-trivial boundaries in configuration space.

Since one hard-core anisotropic particle already poses mathematical challenges and, ordinarily, natural systems comprise large ensembles of anisotropic particles, it is easy to see that their study is substantially more challenging. This explains the dearth of macroscopic PDE models systematically derived from underlying dynamics and the popularity of computational and phenomenological approaches to incorporate anisotropic interactions in PDE models. Phenomenological models have been widely used in the context of polymer and liquid crystals theory. These include the so-called tube theory [25], which assumes polymers as rigid filaments that, under crowding, move along a tube formed by the surrounding polymers, as well as the Landau-de Gennes Q-tensor theory for nematic liquid crystals [26], which represents polar molecules via a continuum order parameter. A lot of work has been dedicated to validating these theories by comparing their predictions with microscopic models with different levels of success [27].

In Mandal *et al.* [28], they consider a system of self-propelled needles, with collisions such that energy and momentum are preserved, and validate the tube theory (they find that the self-diffusion coefficient of a needle increases with concentration, in contrast to that of hard spheres [29]).

In this article, we focus on, possibly, the simplest hard-core anisotropic system, namely, that of N Brownian needles of length ϵ with non-overlapping constraints in two dimensions. By using matched asymptotic expansions, we systematically derive a macroscopic PDE model in the asymptotic regime $\epsilon^2 N \ll 1$. To our knowledge, this is the first systematic derivation for such a system. We take an approach similar to [2], in which the authors consider a system of N Brownian hard disks of diameter ϵ under a drift $\mathbf{f}(\mathbf{x})$ in two spatial dimensions. Under the assumption that the volume fraction of the particles is small, the one-particle probability density $\rho(\mathbf{x}, t)$ satisfies the nonlinear diffusion equation (equation (11) of reference [2])

$$\frac{\partial \rho}{\partial t}(\mathbf{x}, t) = \nabla_{\mathbf{x}} \cdot \{[1 + \pi (N-1)\, \epsilon^2 \rho] \nabla_{\mathbf{x}} \rho - \mathbf{f}(\mathbf{x}) \rho\}, \tag{1.1}$$

in $\mathbb{R}^2$. The goal of this article is to derive an analogous PDE to (1.1) for the one-particle density $p(\mathbf{x}, \theta, t)$ describing the probability of a needle with centre at $\mathbf{x}$ and orientation θ at time t.

The structure of this article is as follows. In §2, we introduce the particle-based model, that is, a system of N Brownian needles with drifts and its associated Fokker–Planck equation describing the whole ensemble probabilistically. Section 3 is devoted to the systematic derivation of the effective model using the method of matched asymptotic expansions. Section 4 is dedicated to systems with high rotational diffusion coefficients, which are shown to inherit striking similarities with the hard-disk model, §5, proposed by [2]. We conclude this article with the space-homogeneous model and, upon performing a linear stability analysis, we find that the system exhibits an isotropic-to-nematic phase transition consistent with Onsager's theory [30].

2. The microscopic model and its associated Fokker–Planck equation

We start by describing the individual-based (microscopic) model. We suppose there are $N \in \mathbb{N}$ identical hard needles of length ϵ distributed in a bounded domain $\Omega \in \mathbb{R}^2$. For $1 \leq i \leq N$, we denote by $\mathbf{X}_i(t) \in \Omega$ the centre of the ith needle and by $\Theta_i(t) \in [0, \pi]$ its orientation. We choose Ω to be the two-dimensional torus $\mathbb{T} = \mathbb{R}/(\pi\mathbb{Z})$, imposing periodic boundary conditions. The π-period is chosen for mathematical convenience, such that $\Upsilon = \Omega \times [0, \pi) = \mathbb{T}^3$. As pointed out in §1, the spatial extension of the needles restricts their ability to move freely in the domain due to non-overlapping constraints, in contrast to a system of point particles.

Each needle evolves according to a translational (resp. rotational) Brownian motion with diffusion constant D_T (resp. D_R) in an external force field $f = (\mathbf{f}_T, f_R)$ that may depend on both the position and orientation of the needle, but not on the other needles. This leads to the system of stochastic differential equations (SDEs)

$$\mathrm{d}\mathbf{X}_i(t) = \sqrt{2D_T}\, \mathrm{d}\mathbf{W}_{T,i}(t) + \mathbf{f}_T(\mathbf{X}_i, \Theta_i)\, \mathrm{d}t \tag{2.1a}$$

and

$$\mathrm{d}\Theta_i(t) = \sqrt{2D_R}\, \mathrm{d}W_{R,i}(t) + f_R(\mathbf{X}_i, \Theta_i)\, \mathrm{d}t, \tag{2.1b}$$

for $1 \leq i \leq N$ and $(\mathbf{X}_i, \Theta_i) \in \Upsilon$. Here, $\mathbf{W}_{T,i}$ and $W_{R,i}$ are standard independent Brownian motions for $1 \leq i \leq N$. In addition, we impose reflective boundary conditions whenever two needles come into contact, thereby introducing a coupling to an otherwise uncoupled system of N SDEs.

It is convenient to consider the *joint probability density* $P_N(\vec{\xi}, t)$ associated to system (2.1), where $\vec{\xi} = (\xi_1, \ldots, \xi_N)$ and $\xi_i = (\mathbf{x}_i, \theta_i)$, for $1 \leq i \leq N$. The density P_N describes the probability of the entire system of N needles being in state $\vec{\xi}$ at time t. It is well known that P_N satisfies the Fokker–Planck

royalsocietypublishing.org/journal/rspa Proc. R. Soc. A 479: 20230076

equation [31]:

$$\partial_t P_N = \nabla_{\vec{x}} \cdot [D_T \nabla_{\vec{x}} P_N - \vec{F}_T(\vec{\xi}) P_N] + \nabla_{\vec{\theta}} \cdot [D_R \nabla_{\vec{\theta}} P_N - \vec{F}_R(\vec{\xi}) P_N], \tag{2.2a}$$

where $\vec{x} = (\mathbf{x}_1, \ldots, \mathbf{x}_N)$, $\vec{\theta} = (\theta_1, \ldots, \theta_N)$, $\vec{F}_T(\vec{\xi}) = (\mathbf{f}_T(\xi_1), \ldots, \mathbf{f}_T(\xi_N))$ and $\vec{F}_R(\vec{\xi}) = (f_R(\xi_1), \ldots, f_R(\xi_N))$. Due to the hard-core interactions between needles, note that (2.2*a*) is not defined on $\vec{\xi} \in \Upsilon^N$ but its perforated form $\Upsilon_\epsilon^N := \Upsilon^N \setminus \mathcal{B}_\epsilon^N$. Here, $\mathcal{B}_\epsilon^N$ denotes the set of *illegal configurations* where at least two needles overlap, i.e.

$$\mathcal{B}_\epsilon^N := \left\{ \vec{\xi} \in (\Upsilon)^N \mid \exists i \neq j \text{ s.t. } \mathcal{N}(\xi_i) \cap \mathcal{N}(\xi_j) \neq \emptyset \right\},$$

where

$$\mathcal{N}(\mathbf{x}, \theta) := \left\{ \vec{x} + \lambda \begin{pmatrix} \cos(\theta) \\ \sin(\theta) \end{pmatrix} \,\middle|\, |\lambda| \leq \frac{\epsilon}{2} \right\}$$

denotes the set of all points belonging to a needle at $(\mathbf{x}, \theta)$.

On $\partial \Upsilon_\epsilon^N$ (corresponding to configurations with at least two needles in contact), we prescribe reflective boundary conditions

$$\begin{bmatrix} D_T \nabla_{\vec{x}} P_N - \vec{F}_T(\vec{\xi}) P_N \\ D_R \nabla_{\vec{\theta}} P_N - F_R(\vec{\xi}) P_N \end{bmatrix} \cdot \vec{n} = 0, \quad \text{on } \partial \Upsilon_\epsilon^N, \tag{2.2b}$$

where $\vec{n} \in \mathcal{S}^{3N-1}$ denotes the unit outward normal on the boundary. Finally, we assume that the initial positions of the particles are identically distributed so that the initial condition $P(\vec{\xi}, 0) = P_0(\vec{\xi})$ is invariant to permutations of the particles' labels.

3. Derivation of the macroscopic model

In the previous section, we have established a connection between the particle-based dynamical system (2.1) and the associated Fokker–Planck equation (2.2*a*), (2.2*b*). We highlight that the dimensionality of both descriptions increases as more needles are added to the system, rendering their analytical or numerical study intractable. This section is dedicated to deriving an effective model in the form of a nonlinear evolution equation for the *one-particle probability density*

$$p(\xi, t) := \int_{\Upsilon_\epsilon^N} P_N(\vec{\xi}, t) \delta(\xi_1 - \xi) \, \mathrm{d}\vec{\xi}. \tag{3.1}$$

In the case of $\epsilon = 0$, the needles become point particles and, as a consequence, their evolutions (2.1) decouple and, for suitable iid initial conditions, we have that

$$P_N(\vec{\xi}, t) = \prod_{i=1}^{N} p(\xi_i, t).$$

In this setting, the first marginal is shown to satisfy the following equation:

$$\partial_t p(\xi, t) = \nabla_{\mathbf{x}} \cdot [D_T \nabla_{\mathbf{x}} p - \mathbf{f}_T(\xi) p] + \partial_\theta [D_R \partial_\theta p - f_R(\xi) p], \tag{3.2}$$

with $t \geq 0$ and $\xi \in \Upsilon$. Unlike point particles, needles of length $\epsilon > 0$ exclude a certain volume in phase space.

Remark 3.1 (Excluded region of a needle). The region in phase space excluded by a needle at ξ_1 is denoted by $B_\epsilon(\xi_1)$ (figure 1). Depending on the relative orientation $\theta := \theta_2 - \theta_1$ between the two needles, the cross-section of B_ϵ for fixed θ range from a line of length $2\epsilon(\theta = 0)$ to a square of

side ϵ ($\theta = \pi/2$). For general θ, the slice is a rhombus of area $\epsilon^2 \sin\theta$ with nodes at

$$\left.\begin{aligned} &\mathbf{x}_A = \mathbf{x}_1 + \frac{\epsilon}{2} R_{\theta_1}(-1+\cos\theta, \sin\theta), \quad \mathbf{x}_B = \mathbf{x}_1 + \frac{\epsilon}{2} R_{\theta_1}(1+\cos\theta, \sin\theta) \\ \text{and} \quad &\mathbf{x}_C = \mathbf{x}_1 + \frac{\epsilon}{2} R_{\theta_1}(1-\cos\theta, -\sin\theta), \quad \mathbf{x}_D = \mathbf{x}_1 + \frac{\epsilon}{2} R_{\theta_1}(-1-\cos\theta, -\sin\theta), \end{aligned}\right\} \tag{3.3}$$

where R_{θ_1} is the rotation matrix

$$R_{\theta_1} = \begin{pmatrix} \cos\theta_1 & -\sin\theta_1 \\ \sin\theta_1 & \cos\theta_1 \end{pmatrix}. \tag{3.4}$$

We denote by $\hat{n}_2$ the outward unit normal on $B_\epsilon(\xi_1)$ (outward of $\Upsilon(\xi_1)$ so it points into the shaded area in figure 1. If the boundary of $B_\epsilon(\xi_1)$ is given by the relation $\chi(\xi_2) = 0$, we have that $\hat{n}_2 \propto \nabla_{\xi_2}\chi$. For example, the top edge $\mathbf{x}_A\mathbf{x}_B$ is given by $\chi(\xi_2) = y_A + \tan\theta_1(x_2 - x_A) - y_2 = 0$, and the normal vector is

$$\hat{n}_2 \propto \nabla_{\xi_2}\chi = \left(\tan\theta_1, 1, \frac{\epsilon}{2}(\cos\theta_2 + \tan\theta_1 \sin\theta_2)\right). \tag{3.5}$$

For $\epsilon > 0$, the equation for the one-particle density $p(\xi_1, t)$ is obtained by integrating (2.2*a*) with respect to $\xi_2, \ldots, \xi_N$ for ξ_1 fixed. The perforations in Υ_ϵ^N lead to boundary integrals for $\xi_i \in B_\epsilon(\xi_1)$ on which the two-particle probability density $P_2(\xi_1, \xi_i, t)$ needs to be evaluated. One can go back to (2.2*a*) and (2.2*b*) and obtain an equation for P_2, which in turn depends on the three-particle probability density P_3. This is known as the BBGKY hierarchy. In this work, we assume that $\phi = \epsilon^2 N \ll 1$ such that this hierarchy can be truncated 'asymptotically'.

We note from remark 3.1 that the volume of $B_\epsilon(\xi_1)$ is $\epsilon^2 \int_0^\pi \sin(\theta)\,\mathrm{d}\theta = 2\epsilon^2$. If $\phi \ll 1$, the volume in Υ_ϵ^N occupied by configurations where two needles are close by is $O(\phi)$, whereas the volume of configurations where three or more needles are nearby is much smaller ($O(\phi^2)$). Hence, it means that, at the leading order, the equation for p coincides with the point particles equation (3.2) and that the first correction appears at $O(\phi)$ and is due to two-needle interactions. Three- and more-needle interactions are higher-order corrections. Therefore, we may neglect three-particle interactions in the equation for $P_2(\xi_1, \xi_2, t)$ and consider

$$\partial_t P_2 = \nabla_{\xi_1} \cdot [D\nabla_{\xi_1} P_2 - f(\xi_1)P_2] + \nabla_{\xi_2} \cdot [D\nabla_{\xi_2} P_2 - f(\xi_2)P_2], \tag{3.6a}$$

in Υ_ϵ^2, where $D = \mathrm{diag}(D_T, D_T, D_R)$ and $f(\xi) = (\mathbf{f}_T(\xi), f_R(\xi))$, together with reflecting boundary conditions

$$[D\nabla_{\xi_1} P_2 - f(\xi_1)P_2] \cdot n_1 + [D\nabla_{\xi_2} P_2 - f(\xi_2)P_2] \cdot n_2 = 0, \tag{3.6b}$$

on $\partial\Upsilon_\epsilon^2$. Here, n_1 (resp. n_2) are the components of the unit normal $\vec{n}$ corresponding to the coordinates of the first (resp. second) needle. It turns out that $n_1 = -n_2$ such that $\vec{n} = \sqrt{2}/2(-\hat{n}_2, \hat{n}_2)$, where $\hat{n}_2$ is defined in remark 3.1.

(a) Evolution of the first marginal

Let $\Upsilon(\xi_1) = \Upsilon \setminus B_\epsilon(\xi_1)$ denote the second particle's phase space given that the first particle is in state ξ_1. From (3.1), we have that $p(\xi_1, t) = \int_{\Upsilon(\xi_1)} P_2(\xi_1, \xi_2, t)\,\mathrm{d}\xi_2$. Integrating (3.6*a*) over $\Upsilon(\xi_1)$ yields

$$\begin{aligned} \partial_t p(\xi_1, t) &= \int_{\Upsilon(\xi_1)} \partial_t P_2(\xi_1, \xi_2, t)\,\mathrm{d}\xi_2 \\ &= \int_{\Upsilon(\xi_1)} \nabla_{\xi_1} \cdot [D\nabla_{\xi_1} P_2 - f(\xi_1)P_2]\,\mathrm{d}\xi_2 + \int_{\Upsilon(\xi_1)} \nabla_{\xi_2} \cdot [D\nabla_{\xi_2} P_2 - f(\xi_2)P_2]\,\mathrm{d}\xi_2. \end{aligned} \tag{3.7}$$

By using Reynold's transport theorem, the first integral becomes

$$\begin{aligned} &\int_{\Upsilon(\xi_1)} \nabla_{\xi_1} \cdot [D\nabla_{\xi_1} P_2 - f(\xi_1)P_2]\,\mathrm{d}\xi_2 \\ &= \nabla_{\xi_1} \cdot [D\nabla_{\xi_1} p - f(\xi_1)p] + \oint_{\partial B_\epsilon(\xi_1)} [f(\xi_1)P_2 - 2D\nabla_{\xi_1} P_2 - D\nabla_{\xi_2} P_2] \cdot \hat{n}_2\,\mathrm{d}S_{\xi_2}. \end{aligned} \tag{3.8}$$

The second integral in (3.7) is

$$\int_{\Upsilon(\xi_1)} \nabla_{\xi_2} \cdot [D\nabla_{\xi_2} P_2 - f(\xi_2)P_2]\,\mathrm{d}\xi_2 = \oint_{\partial B_\epsilon(\xi_1)} [D\nabla_{\xi_2} P_2 - f(\xi_2)P_2] \cdot \hat{n}_2\,\mathrm{d}S_{\xi_2}. \tag{3.9}$$

By substituting (3.8) and (3.9) into (3.7) and using the boundary condition (3.6*b*), we obtain

$$\partial_t p(\xi_1, t) = \nabla_{\xi_1} \cdot [D\nabla_{\xi_1} p - f(\xi_1)p] + I, \tag{3.10}$$

where the collision integral I is

$$I = -\oint_{\partial B_\epsilon(\xi_1)} D(\nabla_{\xi_1} P_2 + \nabla_{\xi_2} P_2) \cdot \hat{n}_2\,\mathrm{d}S_{\xi_2}. \tag{3.11}$$

The evolution equation (3.10) for the first marginal p still depends on the joint probability density function P_2. A common approach to overcome this is to use a closure assumption, for instance, the mean-field approximation, $P_2(\xi_1, \xi_2, t) = p(\xi_1, t)p(\xi_2, t)$. However, such an approach ignores correlations between both particles, and it is not suitable for systems of strongly interacting particles with short-range repulsive interactions such as hard needles. Instead, we employ the method of matched asymptotics to compute the collision integral I systematically.

(b) Matched asymptotics expansions

We introduce a partition of the domain $\Upsilon(\xi_1)$ consisting of an *inner region*, when the two needles are close to each other, $||x_1 - x_2||_2 \sim \epsilon$, and an *outer region*, when the two needles are far apart, $||\mathbf{x}_1 - \mathbf{x}_2|| \gg \epsilon$. In the outer region, we suppose that particles are independent at leading order, whereas we consider their correlation in the inner region.

In the outer region, we define $P_{out}(\xi_1, \xi_2, t) = P_2(\xi_1, \xi_2, t)$. Then by independence, the two-particle density function is[1]

$$P_{out}(\xi_1, \xi_2, t) = p(\xi_1, t)p(\xi_2, t) + \epsilon P^{(1)}_{out}(\xi_1, \xi_2, t) + \cdots. \tag{3.12}$$

In the inner region, we introduce the *inner variables* $\tilde{\xi}_1 = (\tilde{\mathbf{x}}_1, \tilde{\theta}_1)$ and $\tilde{\xi} = (\tilde{\mathbf{x}}, \tilde{\theta})$, defined as follows:

$$\left.\begin{aligned} &\mathbf{x}_1 = \tilde{\mathbf{x}}_1, \quad \mathbf{x}_2 = \tilde{\mathbf{x}}_1 + \epsilon R_{\theta_1}\tilde{\mathbf{x}} \\ \text{and} \qquad &\theta_1 = \tilde{\theta}_1, \quad \theta_2 = \tilde{\theta}_1 + \tilde{\theta}, \end{aligned}\right\} \tag{3.13}$$

and the inner function $\tilde{P}(\tilde{\xi}_1, \tilde{\xi}, t) = P_2(\xi_1, \xi_2, t)$. The coordinates $(\tilde{\mathbf{x}}, \tilde{\theta})$ define the configuration of the second needle relative to the first. The excluded volume $B_\epsilon(\xi_1)$ becomes $B_1(0)$ in inner variables. In the $\tilde{\xi}$-space, this is now a volume centred at the origin with two horizontal sides (figure 1 and remark 3.1). Using that $\tilde{\mathbf{x}} = \epsilon^{-1} R^T_{\theta_1}(\mathbf{x}_2 - \mathbf{x}_1)$, the derivatives transform according to

$$\begin{aligned} &\nabla_{\mathbf{x}_1} \to \nabla_{\tilde{\mathbf{x}}_1} - \epsilon^{-1} R_{\theta_1} \nabla_{\tilde{\mathbf{x}}}, \qquad \nabla_{\mathbf{x}_2} \to \epsilon^{-1} R_{\theta_1} \nabla_{\tilde{\mathbf{x}}}, \\ &\partial_{\theta_1} \to \partial_{\tilde{\theta}_1} - \partial_{\tilde{\theta}} + \tilde{y}\partial_{\tilde{x}} - \tilde{x}\partial_{\tilde{y}}, \quad \partial_{\theta_2} \to \partial_{\tilde{\theta}}. \end{aligned}$$

In terms of the inner variables, (3.6*a*) reads

$$\begin{aligned} \epsilon^2 \partial_t \tilde{P} = {} & 2D_T \Delta_{\tilde{\mathbf{x}}} \tilde{P} \\ & - \epsilon(2D_T \nabla_{\tilde{\mathbf{x}}_1} \cdot (R_{\theta_1} \nabla_{\tilde{\mathbf{x}}} \tilde{P}) + \nabla_{\tilde{\mathbf{x}}} \cdot \{R_{\theta_1}[\mathbf{f}_T(\tilde{\mathbf{x}}_1 + \epsilon\tilde{\mathbf{x}}, \tilde{\theta}_1 + \tilde{\theta}) - \mathbf{f}_T(\tilde{\xi}_1)]\tilde{P}\}) \\ & + \epsilon^2 \Big\{ \nabla_{\tilde{\mathbf{x}}_1} \cdot [D_T \nabla_{\tilde{\mathbf{x}}_1} \tilde{P} - \mathbf{f}_T(\tilde{\xi}_1)\tilde{P}] + D_R[(\partial_{\tilde{\theta}_1} - \partial_{\tilde{\theta}} + \tilde{y}\partial_{\tilde{x}} - \tilde{x}\partial_{\tilde{y}})^2 + \partial^2_{\tilde{\theta}}]\tilde{P} \\ & \quad - (\partial_{\tilde{\theta}_1} - \partial_{\tilde{\theta}} + \tilde{y}\partial_{\tilde{x}} - \tilde{x}\partial_{\tilde{y}})[f_R(\tilde{\xi}_1)\tilde{P}] - \partial_{\tilde{\theta}}[f_R(\tilde{\mathbf{x}}_1 + \epsilon\tilde{\mathbf{x}}, \tilde{\theta}_1 + \tilde{\theta})\tilde{P}] \Big\}. \end{aligned} \tag{3.14}$$

In order to write the boundary condition (3.6*b*) in terms of the inner variables, we need to determine how the normal $\hat{n}_2$ changes under the transformation. Following the procedure in

[1]Independence only tells us that $P_{out}(\xi_1, \xi_2, t) \sim q(\xi_1, t)q(\xi_2, t)$ for some function q, but the normalization condition on P_2 implies $p = q + O(\epsilon)$.

remark 3.1, we have $\nabla_{\tilde{\xi}_2}\chi \to (\epsilon^{-1}R_{\theta_1}\nabla_{\tilde{\mathbf{x}}}\tilde{\chi}, \partial_{\tilde{\theta}}\tilde{\chi})$, where $\tilde{\chi}(\tilde{\xi}) = 0$ describes the boundary in inner variables. Therefore,

$$\hat{n}_2 \to (R_{\theta_1}\tilde{\mathbf{n}}, \epsilon\tilde{n}_\theta). \tag{3.15}$$

For example, the top edge $\mathbf{x}_A\mathbf{x}_B$ becomes $\tilde{\chi} = \sin(\tilde{\theta}) - \tilde{y} = 0$ and the normal vector in the inner variables is $\tilde{n} = (\tilde{\mathbf{n}}, \tilde{n}_\theta) \propto \nabla_{\tilde{\mathbf{x}}}\tilde{\chi} = (0, -1, \cos\tilde{\theta})$. Using (3.15) and $n_1 = -n_2$ as pointed out earlier, the no-flux boundary condition (3.6*b*) becomes

$$\begin{aligned} 0 = {} & \{2D_T R_{\theta_1}\nabla_{\tilde{\mathbf{x}}}\tilde{P} - \epsilon D_T \nabla_{\tilde{\mathbf{x}}_1}\tilde{P} - \epsilon[\mathbf{f}_T(\tilde{\mathbf{x}}_1 + \epsilon\tilde{\mathbf{x}}, \tilde{\theta}_1 + \tilde{\theta}) - \mathbf{f}_T(\tilde{\xi}_1)]\tilde{P}\} \cdot R_{\theta_1}\tilde{\mathbf{n}} \\ & + \epsilon^2\{D_R\big[2\partial_{\tilde{\theta}}\tilde{P} - \partial_{\tilde{\theta}_1}\tilde{P} + \tilde{x}\partial_{\tilde{y}}\tilde{P} - \tilde{y}\partial_{\tilde{x}}\tilde{P}\big] - \big[f_R(\tilde{\mathbf{x}}_1 + \epsilon\tilde{\mathbf{x}}, \tilde{\theta}_1 + \tilde{\theta}) - f_R(\tilde{\xi}_1)\big]\tilde{P}\}\tilde{n}_\theta, \end{aligned} \tag{3.16}$$

for $\tilde{\xi} \in \partial B_1(0)$. Finally, we impose the *matching boundary condition* to ensure that, as the two needles become further apart and enter the outer region, the inner solution $\tilde{P}$ will match with the outer solution P_{out}. Expanding (3.12) in the inner variables,

$$\begin{aligned} \tilde{P} & \sim p(\tilde{\mathbf{x}}_1, \tilde{\theta}_1, t)p(\tilde{\mathbf{x}}_1 + \epsilon R_{\theta_1}\tilde{\mathbf{x}}, \tilde{\theta}_1 + \tilde{\theta}, t) + \epsilon P^{(1)}_{out}(\tilde{\mathbf{x}}_1, \tilde{\theta}_1, \tilde{\mathbf{x}}_1 + \epsilon R_{\theta_1}\tilde{\mathbf{x}}, \tilde{\theta}_1 + \tilde{\theta}, t) \\ & \sim pp^+ + \epsilon[pR_{\theta_1}\tilde{\mathbf{x}} \cdot \nabla_{\tilde{\mathbf{x}}_1}p^+ + P^{(1)}_{out}(\tilde{\mathbf{x}}_1, \tilde{\theta}_1, \tilde{\mathbf{x}}_1, \tilde{\theta}_1 + \tilde{\theta}, t)], \quad \text{as } |\tilde{\mathbf{x}}| \to \infty, \end{aligned} \tag{3.17}$$

where $p := p(\tilde{\mathbf{x}}_1, \tilde{\theta}_1, t)$ and $p^+ := p(\tilde{\mathbf{x}}_1, \tilde{\theta}_1 + \tilde{\theta}, t)$.

We look for a solution of (3.14), (3.16) and (3.17) of the form $\tilde{P} = \tilde{P}^{(0)} + \epsilon\tilde{P}^{(1)} + \cdots$. The leading-order problem is

$$\begin{cases} \Delta_{\tilde{\mathbf{x}}}\tilde{P}^{(0)} = 0, & \\ R_{\theta_1}\nabla_{\tilde{\mathbf{x}}}\tilde{P}^{(0)} \cdot R_{\theta_1}\tilde{\mathbf{n}} = 0, & \tilde{\xi} \in \partial B_1(0), \\ \tilde{P}^{(0)} \sim pp^+, & |\tilde{\mathbf{x}}| \sim \infty. \end{cases} \tag{3.18}$$

This is a problem in the inner spatial variables $\tilde{\mathbf{x}}$, and that $\tilde{\mathbf{x}}_1$, $\tilde{\theta}_1$ and $\tilde{\theta}$ can be regarded as parameters. In particular, (3.18) is defined for $\tilde{\mathbf{x}} \in \mathbb{R}^2 \setminus \mathcal{R}_{\tilde{\theta}}$, where $\mathcal{R}_{\tilde{\theta}}$ denotes the rhombus corresponding to slicing the excluded volume $B_1(0)$ at $\tilde{\theta}$ (figure 1). The solution of (3.18) is

$$\tilde{P}^{(0)} = pp^+. \tag{3.19}$$

By using (3.19) and expanding $\mathbf{f}_T$, the $O(\epsilon)$ problem reads

$$\left.\begin{aligned} & \Delta_{\tilde{\mathbf{x}}}\tilde{P}^{(1)} = 0, && \tilde{\mathbf{x}} \in \mathbb{R}^2 \setminus \mathcal{R}_{\tilde{\theta}}, \\ & R_{\theta_1}\nabla_{\tilde{\mathbf{x}}}\tilde{P}^{(1)} \cdot R_{\theta_1}\tilde{\mathbf{n}} = \tfrac{1}{2}\left[\nabla_{\tilde{\mathbf{x}}_1}(pp^+) + \tfrac{(pp^+)}{D_T}(\mathbf{f}_T^+ - \mathbf{f}_T)\right] \cdot R_{\theta_1}\tilde{\mathbf{n}}, && \tilde{\mathbf{x}} \in \partial\mathcal{R}_{\tilde{\theta}} \\ \text{and} \quad & \tilde{P}^{(1)} \sim p\nabla_{\tilde{\mathbf{x}}_1}p^+ \cdot R_{\theta_1}\tilde{\mathbf{x}} + P^{(1)}_{out}(\tilde{\mathbf{x}}_1, \tilde{\theta}_1, \tilde{\mathbf{x}}_1, \tilde{\theta}_1 + \tilde{\theta}, t), && |\tilde{\mathbf{x}}| \sim \infty, \end{aligned}\right\} \tag{3.20}$$

where $\mathbf{f}_T := \mathbf{f}_T(\tilde{\mathbf{x}}_1, \tilde{\theta}_1)$ and $\mathbf{f}_T^+ := \mathbf{f}_T(\tilde{\mathbf{x}}_1, \tilde{\theta}_1 + \tilde{\theta})$. We can rewrite problem (3.20) as follows:

$$\begin{cases} \Delta_{\tilde{\mathbf{x}}}\tilde{P}^{(1)} = 0, & \tilde{\mathbf{x}} \in \mathbb{R}^2 \setminus \mathcal{R}_{\tilde{\theta}}, \\ \nabla_{\tilde{\mathbf{x}}}\tilde{P}^{(1)} \cdot \tilde{\mathbf{n}} = R^T_{\theta_1}\mathbf{A} \cdot \tilde{\mathbf{n}}, & \tilde{\mathbf{x}} \in \partial\mathcal{R}_{\tilde{\theta}}, \\ \tilde{P}^{(1)} \sim R^T_{\theta_1}\mathbf{B}_\infty \cdot \tilde{\mathbf{x}} + C_\infty, & |\tilde{\mathbf{x}}| \sim \infty, \end{cases} \tag{3.21}$$

where $\mathbf{A}$, $\mathbf{B}_\infty$ and C_∞ are functions of $\tilde{\mathbf{x}}_1, \tilde{\theta}_1, \tilde{\theta}$ and t only and given by

$$\left.\begin{aligned} & \mathbf{A} = \frac{1}{2}\left[\nabla_{\tilde{\mathbf{x}}_1}(pp^+) + \frac{pp^+}{D_T}(\mathbf{f}_T^+ - \mathbf{f}_T)\right], \\ & \mathbf{B}_\infty = p\nabla_{\tilde{\mathbf{x}}_1}p^+ \\ \text{and} \quad & C_\infty = P^{(1)}_{out}(\tilde{\mathbf{x}}_1, \tilde{\theta}_1, \tilde{\mathbf{x}}_1, \tilde{\theta}_1 + \tilde{\theta}, t). \end{aligned}\right\} \tag{3.22}$$

The solution to (3.21) is given by

$$\tilde{P}^{(1)} = R^T_{\theta_1}\mathbf{A} \cdot \tilde{\mathbf{x}} + R^T_{\theta_1}\mathbf{B} \cdot \mathbf{u} + C_\infty, \tag{3.23}$$

where $\mathbf{B} := \mathbf{B}_\infty - \mathbf{A}$ and $\mathbf{u} = (u_1, u_2)$ satisfy the following problems:

$$\begin{cases} \Delta_{\tilde{\mathbf{x}}} u_1 = 0, & \tilde{\mathbf{x}} \in \mathbb{R}^2 \setminus \mathcal{R}_{\tilde{\theta}}, \\ \nabla_{\tilde{\mathbf{x}}} u_1 \cdot \tilde{\mathbf{n}} = 0, & \tilde{\mathbf{x}} \in \partial\mathcal{R}_{\tilde{\theta}}, \\ u_1 \sim \tilde{x}, & |\tilde{\mathbf{x}}| \sim \infty, \end{cases} \tag{3.24}$$

and

$$\begin{cases} \Delta_{\tilde{\mathbf{x}}} u_2 = 0, & \tilde{\mathbf{x}} \in \mathbb{R}^2 \setminus \mathcal{R}_{\tilde{\theta}}, \\ \nabla_{\tilde{\mathbf{x}}} u_2 \cdot \tilde{\mathbf{n}} = 0, & \tilde{\mathbf{x}} \in \partial\mathcal{R}_{\tilde{\theta}}, \\ u_2 \sim \tilde{y}, & |\tilde{\mathbf{x}}| \sim \infty. \end{cases} \tag{3.25}$$

Thus, we have reduced the inner problem (3.20) to two problems for $u_1(\tilde{\mathbf{x}})$ and $u_2(\tilde{\mathbf{x}})$ that only depend on $\tilde{\theta}$ through their domain of definition, namely, the exterior of a rhombus whose tilting depends on $\tilde{\theta}$ (figure 1). Problems (3.24) and (3.25) are solved via conformal mapping in appendix A.

(c) Collision integral

In this subsection, we go back to the integrated equation (3.10) and use the inner solution $\tilde{P}$ to evaluate the collision integral I in (3.11). By transforming (3.11) to inner variables, we obtain

$$I = -\epsilon D_T \oint_{\partial B_1(0)} \nabla_{\tilde{\mathbf{x}}_1} \tilde{P} \cdot R_{\theta_1} \tilde{\mathbf{n}} \, \mathrm{d}S_{\tilde{\xi}} - \epsilon^2 D_R \oint_{\partial B_1(0)} (\partial_{\tilde{\theta}_1} \tilde{P} + \tilde{y}\partial_{\tilde{x}} \tilde{P} - \tilde{x}\partial_{\tilde{y}} \tilde{P}) \tilde{n}_{\tilde{\theta}} \, \mathrm{d}S_{\tilde{\xi}}, \tag{3.26}$$

using (3.13) and (3.15).

We evaluate (3.26) by breaking I in powers of ϵ, $I = I^{(0)} + \epsilon I^{(1)} + \cdots$. Clearly, $I^{(0)} = 0$. The first-order integral is

$$I^{(1)} = -D_T \oint_{\partial B_1(0)} R_{\theta_1}^T \nabla_{\tilde{\mathbf{x}}_1} \tilde{P}^{(0)} \cdot \tilde{\mathbf{n}} \, \mathrm{d}S_{\tilde{\xi}} = 0,$$

using that $\tilde{P}^{(0)}$ is independent of $\tilde{\mathbf{x}}$, see (3.19), and that we are integrating the normal of a closed curve (for $\tilde{\theta}$ fixed). At the next order, we have

$$I^{(2)} = -D_T \underbrace{\oint_{\partial B_1(0)} R_{\theta_1}^T \nabla_{\tilde{\mathbf{x}}_1} \tilde{P}^{(1)} \cdot \tilde{\mathbf{n}} \, \mathrm{d}S_{\tilde{\xi}}}_{I_{\tilde{\mathbf{x}}}} - D_R \underbrace{\oint_{\partial B_1(0)} \partial_{\tilde{\theta}_1} \tilde{P}^{(0)} \tilde{n}_{\tilde{\theta}} \, \mathrm{d}S_{\tilde{\xi}}}_{I_{\tilde{\theta}}}, \tag{3.27}$$

using again that $\tilde{P}^{(0)}$ is independent of $\tilde{\mathbf{x}}$, making the terms $\tilde{y}\partial_{\tilde{x}} \tilde{P}^{(0)} - \tilde{x}\partial_{\tilde{y}} \tilde{P}^{(0)}$ vanish in the second integral. The latter can be further simplified to

$$I_{\tilde{\theta}} = -\int_{B_1(0)} \partial_{\tilde{\theta}} \partial_{\tilde{\theta}_1} (pp^+) \, \mathrm{d}\tilde{\xi} = -\partial_{\tilde{\theta}_1} \int_0^\pi \partial_{\tilde{\theta}} (pp^+) \int_{\mathcal{R}_{\tilde{\theta}}} \mathrm{d}\tilde{\mathbf{x}} \, \mathrm{d}\tilde{\theta} = -\partial_{\tilde{\theta}_1} \int_0^\pi \sin\tilde{\theta} \, \partial_{\tilde{\theta}} (pp^+) \, \mathrm{d}\tilde{\theta}. \tag{3.28}$$

In the first equality, we have applied the divergence theorem to $(0, 0, \partial_{\tilde{\theta}_1} \tilde{P}^{(0)})$. In the last equality, we have used that $\mathcal{R}_{\tilde{\theta}}$ is the rhombus tilted by angle $\tilde{\theta}$ in inner variables, which has area $\sin\tilde{\theta}$ (remark 3.1). The integral $I_{\tilde{\mathbf{x}}}$ in (3.27) can be rewritten as follows:

$$I_{\tilde{\mathbf{x}}} = \int_0^\pi \int_{\partial\mathcal{R}_{\tilde{\theta}}} R_{\theta_1}^T \nabla_{\tilde{\mathbf{x}}_1} \tilde{P}^{(1)} \cdot \tilde{\mathbf{n}} \, \mathrm{d}S_{\tilde{\mathbf{x}}} \, \mathrm{d}\tilde{\theta} = \int_0^\pi J(\tilde{\mathbf{x}}_1, \tilde{\theta}_1, \tilde{\theta}) \, \mathrm{d}\tilde{\theta}, \tag{3.29}$$

with $J = \int_{\partial\mathcal{R}_{\tilde{\theta}}} R_{\theta_1}^T \nabla_{\tilde{\mathbf{x}}_1} \tilde{P}^{(1)} \cdot \tilde{\mathbf{n}} \, \mathrm{d}S_{\tilde{\mathbf{x}}}$. By using the expression for $\tilde{P}^{(1)}$ in (3.23), we find that (appendix B)

$$J = -\nabla_{\tilde{\mathbf{x}}_1} \cdot (\sin\tilde{\theta}\mathbf{A} + M(\tilde{\theta}_1, \tilde{\theta})\mathbf{B}), \tag{3.30}$$

where $M(\tilde{\theta}_1, \tilde{\theta}) = R_{\theta_1} T(\tilde{\theta}) R_{\theta_1}^T$ with $T(\tilde{\theta})$ the symmetric 2×2 matrix (B 10) whose entries are plotted in figure 2. The matrix $T(\tilde{\theta})$ is positive definite and contains information on the effect of the excluded volume due to a horizontal needle on a second needle with orientation $\tilde{\theta}$. We observe that: for $\tilde{\theta} = \pi/2$, the diagonal terms are equal while the cross-terms are zero, as expected, since

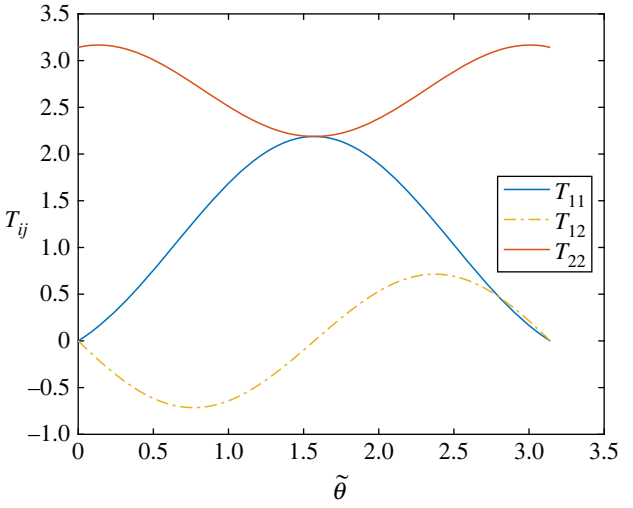

Figure 2. Values T_{11}, T_{12} and T_{22} in (B 10) as a function of $\tilde{\theta}$.

the excluded region is symmetric (a square). For $\tilde{\theta} = 0, \pi$, the needle is 'invisible' to the horizontal flow ($T_{11} = 0$) and the effect on the vertical flow is maximal (T_{22} largest).

Finally, by combining (3.28), (3.29) and (3.30), we find that the leading-order contribution to the collision integral is

$$I = -\epsilon^2 \left(D_T \int_0^\pi J \, \mathrm{d}\tilde{\theta} + D_R I_{\tilde{\theta}} \right) = \epsilon^2 \nabla_{\tilde{\xi}_1} \cdot \int_0^\pi D[\sin\tilde{\theta}\mathbf{A} + M(\tilde{\theta}_1, \tilde{\theta})\mathbf{B}, \sin\tilde{\theta}\,\partial_{\tilde{\theta}}(pp^+)] \, \mathrm{d}\tilde{\theta}. \tag{3.31}$$

(d) A nonlinear non-local diffusion equation

By inserting the collision integral (3.31) into (3.10), we find that the integrated Fokker–Planck equation for $N = 2$ is expressed as follows:

$$\partial_t p = \nabla_{\xi_1} \cdot \left\{ D\nabla_{\xi_1} p - f(\xi_1)p + \epsilon^2 \int_0^\pi D[\sin\theta\mathbf{A} + M(\theta_1, \theta)\mathbf{B}, \sin\theta\,\partial_\theta(pp^+)] \, \mathrm{d}\theta \right\}. \tag{3.32}$$

The extension from two to N needles is straightforward up to $O(\epsilon^2)$ since only pairwise interactions need to be considered at this order. Noting that the first needle has $(N-1)$ inner regions, one with each of the remaining needles, the marginal density for N needles satisfies

$$\partial_t p = \nabla_{\xi_1} \cdot \left\{ D\nabla_{\xi_1} p - f(\xi_1)p + \epsilon^2 (N-1) D \int_0^\pi Q(\theta, p) \, \mathrm{d}\theta \right\}, \tag{3.33a}$$

where $D = \mathrm{diag}(D_T, D_T, D_R)$, $f(\xi_1) = (\mathbf{f}_T(\xi_1), f_R(\xi_1)$, and $Q = (\mathbf{Q}_T, Q_R)$ is given by

$$\mathbf{Q}_T(\theta, p, p^+) = \sin\theta\mathbf{A} + M(\theta_1, \theta)\mathbf{B} \quad \text{and} \quad Q_R(\theta, p, p^+) = \sin\theta p \partial_\theta p^+. \tag{3.33b}$$

In (3.33), $p = p(\mathbf{x}_1, \theta_1, t)$, $p^+ = p(\mathbf{x}_1, \theta_1 + \theta, t)$ and $M(\theta_1, \theta) = R_{\theta_1} T(\theta) R_{\theta_1}^T$, where R_{θ_1} is the rotation matrix by θ_1 (3.4) and $T(\theta)$ is the matrix defined in (B 10) (figure 2), and

$$\left.\begin{aligned} \mathbf{A} &= \frac{1}{2}\left[\nabla_{\mathbf{x}_1}(pp^+) + \frac{(pp^+)}{D_T}(\mathbf{f}_T^+ - \mathbf{f}_T) \right] \\ \text{and} \qquad \mathbf{B} &= \frac{1}{2}\left[p\nabla_{\mathbf{x}_1} p^+ - p^+ \nabla_{\mathbf{x}_1} p + \frac{(pp^+)}{D_T}(\mathbf{f}_T - \mathbf{f}_T^+) \right]. \end{aligned}\right\} \tag{3.33c}$$

The nonlinearities in (3.33) encompass the effect that the non-overlap constraint between needles has on the macroscopic dynamics. In particular, we note that the interactions are local in space but non-local in angle. The integrands $\mathbf{Q}_T$ and Q_R vanish for $\theta = 0$ (as two parallel needles exclude

no volume in phase space), while for $\theta \in (0,\pi)$, they include a series of quadratic terms involving p, p^+ and their derivatives. The interaction in orientation is of mean-field type (see I_R), where only the 'cross-diffusion' term $p\partial_{\theta_1}p^+$ appears, whereas in space we obtain full cross-diffusion terms $p\nabla_{\mathbf{x}_1}p^+$ and $p^+\nabla_{\mathbf{x}_1}p$ as well as a drift-difference term (see $\mathbf{I}_T$), as in the case of mixtures of hard spheres [29]. To give some intuition on their role, consider the kernel $\mathbf{Q}_T$ for $\theta = \pi/2$ (perpendicular needles). This is the only value for which T is a multiple of the identity (see (B 10)), $T(\pi/2) = \mu I_2$ with $\mu \approx 2.18$. Thus, $M(\theta_1,\theta)\mathbf{B} \equiv \mu\mathbf{B}$ and the integrand simplifies to

$$\mathbf{Q}_T(\pi/2,p,p^+) = \mathbf{A} + \mu\mathbf{B} = \frac{1}{2}\left[(\mu+1)p\nabla_{\mathbf{x}_1}p^+ - (\mu-1)\left(p^+\nabla_{\mathbf{x}_1}p - \frac{\mathbf{f}_T - \mathbf{f}_T^+}{D_T}\,pp^+\right)\right].$$

In this form, one may readily compare it with the nonlinear terms arising from the interactions between two types of hard-sphere particles of diameter ϵ (cf. equation (22) in [29])

$$\mathbf{Q}_T(p,p^+) = \frac{\pi}{2}\left[3p\nabla_{\mathbf{x}_1}p^+ - p^+\nabla_{\mathbf{x}_1}p + \frac{\mathbf{f}_T - \mathbf{f}_T^+}{D_T}\,pp^+\right].$$

Thus, we observe the same structure with an 'effective drift' $p\nabla_{\mathbf{x}_1}p^+$ due to gradients of the other species, a reduced diffusion $p^+\nabla_{\mathbf{x}_1}p$ due to concentrations of the other species, and a quadratic drift adjustment with the same relative strength and sign in both needles and hard-spheres cases. The size of the coefficients is larger for hard spheres ($3\pi/2$ and $\pi/2$) than for needles ($(\mu\pm1)/2$), as expected given their excluded volume in this specific needles configuration (π versus 1).

Remark 3.2 (Active Brownian needles). We note that our model (3.33) may be used to describe a system of N active needles similar to that considered in [28] (except that they use the θ-dependent diffusion tensor $\hat{D}$ in (4.2)). In particular, consider $f_R = 0$ and $f_T(\mathbf{x},\theta) = v_0\mathbf{e}(\theta)$ with $\mathbf{e}(\theta) = (\cos\theta,\sin\theta)$ in (2.1), such that needles drift along their orientation θ at constant velocity v_0. This implies that we must now distinguish between a needle's head and tail as its orientation θ determines the direction of the drift in position; i.e. we must extend the range of θ to $[0,2\pi)$. Since the excluded volume between two needles is invariant under switching heads and tails, the terms in (3.33) that describe the excluded volume, namely, $\sin\theta$ and $M(\theta_1,\theta)$ in (3.33*b*), must be extended to $[0,2\pi)$ as $|\sin\theta|$ and $\tilde{M}(\theta_1,\theta)$, respectively, where $\tilde{M}(\theta_1,\theta) = M(\theta_1,\theta)$ for $\theta\in[0,\pi)$ and $\tilde{M}(\theta_1,\theta) = M(\theta_1,\theta-\pi)$ for $\theta\in[\pi,2\pi)$. Then (3.33) becomes

$$\partial_t p = \nabla_{\mathbf{x}_1}\cdot\left[D_T\nabla_{\mathbf{x}_1}p - v_0\mathbf{e}(\theta_1)p + \phi\int_0^{2\pi}\tilde{Q}_T(\theta,p)\,\mathrm{d}\theta\right] + D_R\partial_{\theta_1}\left[\partial_{\theta_1}p + \phi p\int_0^{2\pi}\tilde{Q}_R(\theta,p)\,\mathrm{d}\theta\right], \quad (3.34)$$

where $\phi = (N-1)\epsilon^2$, with

$$\begin{aligned}\tilde{Q}_T(\theta,p) &= \frac{D_T}{2}[(\tilde{M}+|\sin\theta|)p\nabla p^+ - (\tilde{M}-|\sin\theta|)p^+\nabla p] + \frac{v_0}{2}(\tilde{M}-|\sin\theta|)pp^+\widehat{\mathbf{e}}\\ &= D_T(\mu^+p\nabla p^+ - \mu^-p^+\nabla p) + v_0\mu^-pp^+\widehat{\mathbf{e}}\end{aligned}$$

and $$\tilde{Q}_R(\theta,p) = |\sin\theta|\partial_\theta p^+,$$

where $\widehat{\mathbf{e}} = \mathbf{e}(\theta_1) - \mathbf{e}(\theta_1+\theta)$ and $\mu^\pm(\theta_1,\theta) = (1/2)(\tilde{M}(\theta_1,\theta)\pm|\sin\theta|)$. Rearranging (3.34) may be cast in a more familiar form in the active matter community (compared with equation (2.29) in [32], corresponding to active Brownian hard disks):

$$\partial_t p + v_0\nabla\cdot[p(1-\phi\rho^-)\mathbf{e}(\theta_1) + \phi\mathbf{m}^-p] = D_T\nabla\cdot[(1-\phi\rho^-)\nabla p + \phi p\nabla\rho^+] + D_R\partial_{\theta_1}(\partial_{\theta_1}p + \phi p\bar{\rho}), \quad (3.35)$$

with 'effective' spatial densities $\rho^\pm$ and $\bar{\rho}$ and magnetization (also known as polarization)

$$\rho^\pm = \int_0^{2\pi}\mu^\pm p^+\,\mathrm{d}\theta, \quad \bar{\rho} = \int_0^{2\pi}\partial_\theta|\sin\theta|p^+\,\mathrm{d}\theta, \quad \mathbf{m}^- = \int_0^{2\pi}\mu^-p^+\mathbf{e}^+\,\mathrm{d}\theta.$$

If the excluded volume between two needles was a constant, then $\rho^\pm \equiv \rho = \int_0^{2\pi}p\,\mathrm{d}\theta$ (the spatial density), $\mathbf{m}^- \equiv \mathbf{m} = \int_0^{2\pi}p\mathbf{e}\,\mathrm{d}\theta$ and the nonlinear flux in orientation ($p\bar{\rho}$) would drop. This is

because this term represents changes in orientation brought by the change in excluded volume with relative orientation.

4. High rotational diffusion limit

In the context of colloidal suspensions, the diffusion coefficients corresponding to the rotational and translational motions (parallel or perpendicular to the needle's axis) are not independent. In particular, by using Stokes' law, we have that [25,33]

$$D_R = \frac{12D_\perp}{\epsilon^2} \quad D_\parallel = 2D_\perp, \tag{4.1}$$

where $D_\perp$ and $D_\parallel$ are the translational diffusion coefficients for perpendicular and parallel motion. This means that, instead of the constant diffusion matrix $D = \mathrm{diag}(D_T, D_T, D_R)$ used in our derivation, we would have an orientation-dependent matrix, i.e.

$$\hat{D}(\theta_1) := \left(\begin{array}{cc|c} & & 0 \\ & R_{\theta_1} & 0 \\ \hline 0 & 0 & 1 \end{array}\right) D = \begin{pmatrix} \cos\theta_1 D_\parallel & -\sin\theta_1 D_\perp & 0 \\ \sin\theta_1 D_\parallel & \cos\theta_1 D_\perp & 0 \\ 0 & 0 & D_R \end{pmatrix}. \tag{4.2}$$

Our derivation can be adapted to allow for a diffusion matrix of this form, resulting in a modified equation for p (in particular, the $\mathbf{Q}_T$ in (3.33b) would change). We omit this generalization here but comment on the asymptotic regime of (4.1), namely, when the rotational diffusion is much larger than the translational diffusion

$$D_R = \frac{D_T}{\epsilon^2}, \tag{4.3}$$

and set $D_T \equiv 1$ in this section. By inserting (4.3) into (3.33a), we have

$$\begin{aligned} \epsilon^2 \partial_t p = {} & \epsilon^2 \nabla_{\mathbf{x}_1} \cdot [\nabla_{\mathbf{x}_1} p - \mathbf{f}_T(\xi_1) p] + \partial_{\theta_1}[\partial_{\theta_1} p - \epsilon^2 f_R(\xi_1) p] \\ & + \epsilon^4 (N-1) \nabla_{\mathbf{x}_1} \cdot \int_0^\pi \mathbf{Q}_T(\theta, p, p^+)\, \mathrm{d}\theta + \epsilon^2 (N-1) \partial_{\theta_1} \int_0^\pi Q_R(\theta, p, p^+)\, \mathrm{d}\theta. \end{aligned} \tag{4.4}$$

We look for a solution of (4.4) of the form $p \sim p_0 + \epsilon^2 p_1 + \cdots$. The leading-order problem gives that $p_0 = p_0(\mathbf{x}_1, t)$, i.e. the leading-order problem is independent of angle. Collecting the $O(\epsilon^2)$-terms in (4.4) yields

$$\partial_t p_0 = \nabla_{\mathbf{x}_1} \cdot [\nabla_{\mathbf{x}_1} p_0 - \mathbf{f}_T(\xi_1) p_0] + \partial_{\theta_1}[\partial_{\theta_1} p_1 - f_R(\xi_1) p_0], \tag{4.5}$$

where we have used that $Q_R(\theta, p_0, p_0^+) \equiv 0$. The $O(\epsilon^4)$ of (4.4) is

$$\begin{aligned} \partial_t p_1 = {} & \nabla_{\mathbf{x}_1} \cdot [\nabla_{\mathbf{x}_1} p_1 - \mathbf{f}_T(\xi_1) p_1] + \partial_{\theta_1}[\partial_{\theta_1} p_2 - f_R(\xi_1) p_1] \\ & + (N-1) \nabla_{\mathbf{x}_1} \cdot \int_0^\pi \mathbf{Q}_T(\theta, p_0, p_0^+)\, \mathrm{d}\theta + (N-1) \partial_{\theta_1} \int_0^\pi Q_R(\theta, p_0, p_1^+)\, \mathrm{d}\theta, \end{aligned} \tag{4.6}$$

noting that $Q_R(\theta, p_1, p_0^+) \equiv 0$. We now write an equation for the spatial density

$$\rho(\mathbf{x}_1, t) := \int_0^\pi (p_0 + \epsilon^2 p_1)\, \mathrm{d}\theta_1.$$

By combining (4.5) and (4.6), and using periodicity in θ_1, we find

$$\partial_t \rho = \nabla_{\mathbf{x}_1} \cdot \left[\nabla_{\mathbf{x}_1} \rho - \int_0^\pi \mathbf{f}_T(\xi_1) p(\xi_1, t)\, \mathrm{d}\theta_1 + \epsilon^2 (N-1) \int_0^\pi \int_0^\pi \mathbf{Q}_T(\theta; p_0, p_0^+)\, \mathrm{d}\theta \mathrm{d}\theta_1 \right]. \tag{4.7}$$

In particular, if we assume that $\mathbf{f}_T$ is independent of angle, then

$$\partial_t \rho = \nabla_{\mathbf{x}_1} \cdot \left[\nabla_{\mathbf{x}_1} \rho - \mathbf{f}_T(\mathbf{x}_1) \rho + \epsilon^2 (N-1) \int_0^\pi \int_0^\pi \mathbf{Q}_T(\theta; p_0, p_0^+)\, \mathrm{d}\theta\, \mathrm{d}\theta_1 \right]. \tag{4.8}$$

By using that $p_0 = p_0^+$ and $\mathbf{f}_T = \mathbf{f}_T^+$, from (3.33$c$), we have that $\mathbf{A} = p \nabla_{\mathbf{x}_1} p$ and $\mathbf{B} = 0$, and hence, $\mathbf{Q}_T = \sin\theta \nabla_{\mathbf{x}_1}(p_0^2)/2$. The double integral on $\mathbf{Q}_T$ is then $\pi \nabla_{\mathbf{x}_1}(p_0^2) \sim (1/\pi) \nabla_{\mathbf{x}_1}(\rho^2)$ using that $\rho =$

$\pi p_0 + O(\epsilon^2)$. We find that (4.8) reduces to

$$\partial_t \rho = \nabla_{\mathbf{x}_1} \cdot \left\{ \left[1 + \frac{2}{\pi}(N-1)\epsilon^2 \rho \right] \nabla_{\mathbf{x}_1} \rho - \mathbf{f}_T(\mathbf{x}_1)\rho \right\}. \tag{4.9}$$

Therefore, we find that the equation satisfied by N needles of length ϵ in the limit of large rotational diffusion is a nonlinear diffusion equation of the same form as the equation (1.1) satisfied by N disks of diameter ϵ. By comparing the two equations, we have that the effective diameter of a needle with very fast rotational diffusion is $\sqrt{2}/\pi$ times its length ϵ. That is, the needle excludes roughly 45% less volume than a disk of diameter ϵ.

5. Space homogeneous solutions

In this section, we consider spatially homogeneous solutions to (3.33), i.e. solutions of the form $p(\xi_1, t) = p(\theta_1, t)$ satisfying

$$D_R^{-1} \partial_t p = \partial_{\theta_1}^2 p + \epsilon^2 (N-1) \partial_{\theta_1} \left(p \int_0^\pi \sin\theta \, \partial_\theta p^+ \, \mathrm{d}\theta \right). \tag{5.1}$$

The integral is

$$\int_0^\pi \sin\theta \, \partial_\theta p^+ \, \mathrm{d}\theta = -\int_0^\pi \cos\theta p(\theta_1 + \theta) \, \mathrm{d}\theta = \int_0^\pi \cos\theta p(\theta_1 - \theta) \, \mathrm{d}\theta = W' * p,$$

where $W(\theta) = \sin(\theta)$. Therefore, the space-homogeneous system of interacting needles of length ϵ is described by a periodic McKean–Vlasov equation with an attractive potential W ([34,35])

$$D_R^{-1} \partial_t p = \partial_{\theta_1}^2 p + \epsilon^2 (N-1) \partial_{\theta_1} (p W' * p). \tag{5.2}$$

We study the linear stability of the homogeneous solution $p_* = 1/\pi$ of (5.2) by considering a perturbation of the form

$$p = p_* + \delta \, \mathrm{e}^{\lambda t} \sum_{n \geq 0} a_n \cos(2n\theta_1) + b_n \sin(2n\theta_1),$$

with $\delta \ll 1$. By inserting this into (5.2), linearizing and keeping terms of $O(\delta)$, we arrive at

$$\lambda = -4n^2 D_R \left(1 - \frac{2\phi n}{(4n^2 - 1)\pi} \right),$$

where $\phi = \epsilon^2 (N-1)$. We look for growing modes by imposing $\lambda > 0$, leading to $2\phi n > (4n^2 - 1)\pi$. The most unstable mode ($n = 1$) leads to linear instability if

$$\phi > \phi_c = \frac{3\pi}{2}. \tag{5.3}$$

Note that, while ϕ represents an effective volume fraction (which would be bounded for isotropic bodies by their close packing densities, e.g. $\phi < 0.74$ for closely packed hard disks in two dimensions), the hard-core needle system admits any $\phi \in [0, \infty)$, with ∞ corresponding to a system of perfectly aligned needles.

It is also worth pointing out that, while our derivation relied on a diluteness assumption $\phi \ll 1$, the critical volume fraction is $\phi_c = O(1)$. Therefore, the aggregation behaviour occurs outside the region of validity of our PDE model (3.33) and, as a by-product, of the space-homogeneous model (5.2). In fact, the value ϕ_c agrees with the bifurcation point of isotropic-nematic transition obtained in [30] using Onsager's theory of orientational order [20]. In particular, Onsager considers the virial expansion of the orientational probability density up to the second virial coefficient (which depends on two-particle interactions, and Onsager obtains for a variety of hard anisotropic particles evaluating the excluded volume for a pair of such particles). While the third- and higher-order virial coefficients are negligible for hard needles in $\mathbb{R}^3$, it is not the case in the present case of two dimensions [30]. Therefore, the value we obtain for ϕ_c should be taken with caution, and indeed, Monte Carlo simulations have found the critical density at the transition to be $\phi_c \approx 7$ [36].

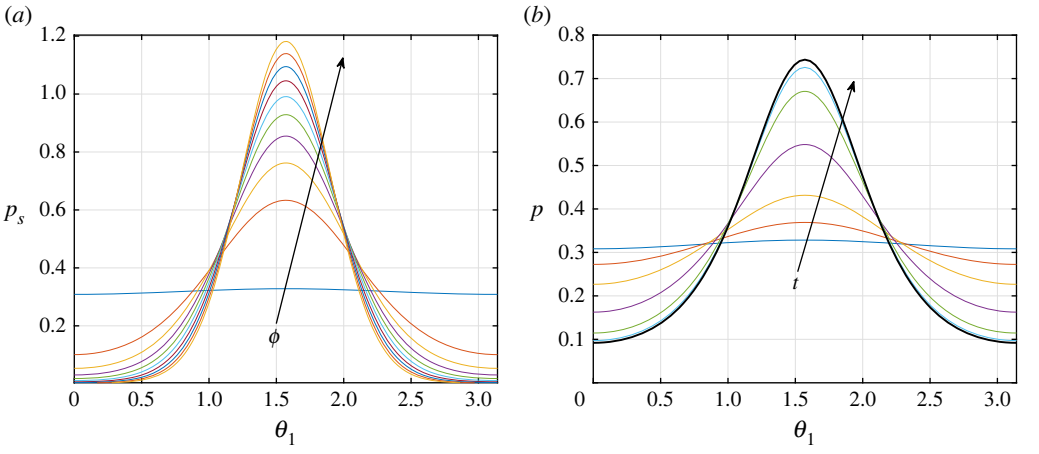

Figure 3. (*a*) Stationary solutions $p_s(\theta_1)$ of the space-homogeneous problem (5.2) for different values of $\phi = (3\pi/2) + k/2$ for $k = 0, \ldots, 10$. Solutions are obtained via a fixed-point iterative scheme using Chebfun [37]. (*b*) Time evolution $p(\theta_1, t)$ for $\phi = 1.1 \times 3\pi/2$ for a small initial perturbation $p_0 = \pi^{-1} - 0.01\cos(2\theta_1)$. Times shown are $t = 0, 4, 6, 8, 10, 12, 20$. At $t = 20$, the solution has already reached the stable equilibrium.

The stationary solutions of (5.2) satisfy

$$\partial_{\theta_1} p_s + \phi p_s W' * p_s = -J,$$

where J is a constant corresponding to the flux of the stationary solution. Without any external forcing, we expect solutions with $J = 0$. By imposing $J = 0$ and integrating, we arrive at

$$p_s(\theta_1) = C \exp\left(\phi \int_0^{\theta_1} (W' * p)(\theta)\, \mathrm{d}\theta\right),$$

where C is a normalization constant such that $\int_0^{\pi} p_s \, \mathrm{d}\theta_1 = 1$. We consider a fixed-point iteration method to compute $p_s(\theta_1)$ above for various values of ϕ. Specifically, given an initialization p_0 (normalized to one), we compute

$$p_{k+1} = C \exp\left(\phi \int_0^{\theta_1} (W' * p_k)(\theta)\, \mathrm{d}\theta\right), \quad \text{for } k = 1, 2, \ldots. \tag{5.4}$$

We initialize the scheme with the most unstable mode from the linear stability analysis ($p_0(\theta_1) = 1/\pi + \delta\cos(2\theta_1)$) and solve (5.4) with Chebfun [37] until it reaches a stationary profile. We consider several values of $\phi \geq 3\pi/2$ so that we expect non-trivial stationary states. Figure 3 shows the results for 10 values of ϕ. We observe that the stationary solution becomes more concentrated as ϕ increases. This means that needles are forced to align more to avoid overlapping as their number increases.

6. Discussion

We have systematically derived an effective PDE model for a system of non-overlapping Brownian needles in two dimensions (3.33). The nonlinearities of the PDE describe the effect of pairwise interactions at the macroscopic level: interactions are non-local in angle (the nonlinearity is of mean-field type, only $p\partial_{\theta_1} p^+$ term) and local in position (full cross-diffusion terms $p\nabla_{\mathbf{x}_1} p^+$ and $p^+\nabla_{\mathbf{x}_1} p$ as well as a drift-difference term appear, consistent with other local-in-space models [29,38]). To gain insight into the behaviour of the PDE model, we consider two simplifications. Firstly, we obtain a reduced PDE for the spatial density in the high-rotational diffusion limit. By comparing the resulting PDE with the effective PDE for hard-core disks in two dimensions, we find that the needles' effective diameter is about 45% of their length. Secondly, we consider

space-homogeneous solutions of the non-local PDE and show they satisfy a well-known McKean–Vlasov equation with an attractive potential in orientation. Notably, we identify instability of the uniform distribution (in angle) for effective packing densities above a critical threshold, see (5.3). Intuitively, we expect this phase transition to occur and arise from the finite-size interactions between needles. Indeed, the instability corresponds to the emergence of a preferred direction of needles to exclude less volume in configuration space in crowded settings. Let us point out that the non-local interaction term in equation (5.2) includes the size of the excluded volume.

In this work, we find that the strength of the nonlinearity in the macroscopic PDE is proportional to the total excluded region volume $(N-1)\,\epsilon^2 \sin\theta$. The form of such nonlinearity is non-trivial in the full PDE (3.33) (due to the spatial interactions). Still, it may have been inferred in the space-homogeneous case (5.1) (in fact, this was the approach taken in [30] using Onsager's free energy functional based on the geometry of the excluded region). A natural question is whether this can be generalized to similar systems. A particularly interesting case is that of Brownian needles in three dimensions, which have zero excluded volume in configuration space (for fixed relative angles, the excluded region is a two-dimensional surface in $\mathbb{R}^3$). If the result from two dimensions were to extend to three dimensions, it would imply that the effective PDE for needles in three dimensions would not 'see' the non-overlapping constraints, at least not to $O(N\epsilon^3)$.

Data accessibility. The data are provided in the electronic supplementary material [39].

Authors' contributions. M.B.: conceptualization, formal analysis, investigation, methodology, software, supervision and writing—original draft; S.J.C.: conceptualization, formal analysis, investigation, methodology, supervision and writing—review and editing; M.S.: formal analysis, investigation, methodology, software, visualization and writing—original draft.

All authors gave final approval for publication and agreed to be held accountable for the work performed therein.

Conflict of interest declaration. We declare we have no competing interests.

Funding. M.B. was supported by a Royal Society University Research Fellowship (grant no. URF/R1/180040).

Acknowledgements. The authors would like to thank Martin Burger for the helpful discussions.

Appendix A. Solution of the first-order inner problem via conformal mapping

We solve problems (3.24) and (3.25) by mapping them to problems in the interior of a circle. We consider the problem for u_1 (3.24); the problem for u_2 follows similarly.

Let D denote the exterior of the rhombus in the z-plane, $D=\mathbb{C}\setminus\mathcal{R}_{\tilde\theta}$, where $z=\tilde x+\imath\tilde y$, and let Γ be its boundary, $\Gamma=\partial\mathcal{R}_{\tilde\theta}$. Let Δ_z denote the Laplacian operator $\partial^2/\partial\tilde x^2+\partial^2/\partial\tilde y^2$. We look for a complex function $w_1: D\to D$ such that the solution we need is given as $u_1=\mathrm{Re}(w_1)$. By the Cauchy–Riemann relations, it follows that the boundary condition $\nabla_{\tilde{\mathbf{x}}}u_1\cdot\tilde{\mathbf{n}}=0$ on Γ is equivalent to imposing that the conjugate harmonic function $\mathrm{Im}(w_1)$ is constant on Γ, e.g. equal to zero. Then, w_1 must satisfy

$$\left.\begin{array}{ll}\Delta_z w_1=0 & \text{in } D,\\ \mathrm{Im}(w_1)=0 & \text{on } \Gamma\\ \text{and} \quad w_1\sim z & \text{at } \infty.\end{array}\right\} \tag{A 1}$$

To proceed with the solution of (A 1), we seek a transformation that simplifies the definition domain. In particular, we look for an analytic function $z=g(\zeta)$ that maps a domain D' of the ζ plane, namely, the interior of the unit disk, to D in the z plane (figure 4). Then the unit circle, denoted by Γ', is mapped into the boundary of the rhombus Γ. This is a Schwarz–Christoffel transformation, given by [40, eq. (4.6)]

$$z=g(\zeta)=a_0+a(\tilde\theta)\int^{\zeta}(1-t^2)^{\tilde\theta/\pi}(1+t^2)^{1-\tilde\theta/\pi}t^{-2}\,\mathrm{d}t, \tag{A 2}$$

where a_0 and $a(\tilde\theta)$ are chosen so that $g(\zeta_k)=z_k$, for $k=A,B,C,D$, where $\zeta_k=\pm1,\pm\imath$ (4). Note that, as we move through the points $A\to B\to C\to D\to A$, we travel the circle counterclockwise, but the rhombus clockwise (so that both curves are positively oriented, i.e. we have the domain to

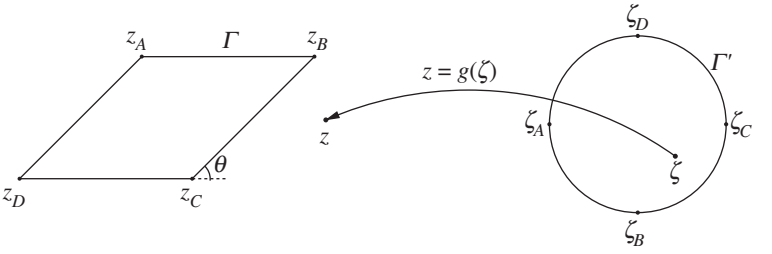

Figure 4. Mapping of the exterior of the unit circle with boundary Γ' into the D of the rhombus with boundary Γ.

our left as we travel on its boundary). We note that $g(\zeta)$ goes to infinity like $-a(\tilde{\theta})/\zeta$ as $\zeta \to 0$. The constant $a(\tilde{\theta})$ is given exactly as follows:

$$a(\tilde{\theta}) = \frac{\alpha}{\beta - \imath\gamma}, \tag{A 3}$$

where α, β and γ are the following real functions of $\tilde{\theta}$:

$$\alpha(\tilde{\theta}) = 2^{1+2\tilde{\theta}/\pi} \sec\tilde{\theta},$$

$$\beta(\tilde{\theta}) = \Gamma(\tfrac{1}{2} - \tfrac{\tilde{\theta}}{\pi})\Gamma(1 + \tfrac{2\tilde{\theta}}{\pi}) \times \left[{}_2\bar{F}_1\left(\frac{1}{2}, \frac{\tilde{\theta}}{\pi}; \frac{3}{2} + \frac{\tilde{\theta}}{\pi}; -1\right) - 2\,{}_2\bar{F}_1\left(-\frac{1}{2}, \frac{\tilde{\theta}}{\pi}; \frac{1}{2} + \frac{\tilde{\theta}}{\pi}; -1\right)\right]$$

and

$$\gamma(\tilde{\theta}) = 16^{\tilde{\theta}/\pi}\,\Gamma(\tfrac{1}{2} + \tfrac{\tilde{\theta}}{\pi})\Gamma(1 - \tfrac{2\tilde{\theta}}{\pi}) \times \left[{}_2\bar{F}_1\left(\frac{1}{2}, -\frac{\tilde{\theta}}{\pi}; \frac{3}{2} - \frac{\tilde{\theta}}{\pi}; -1\right) + 2\,{}_2\bar{F}_1\left(-\frac{1}{2}, -\frac{\tilde{\theta}}{\pi}; \frac{1}{2} - \frac{\tilde{\theta}}{\pi}; -1\right)\right],$$

where ${}_2\bar{F}_1(a, b; c; z) = {}_2F_1(a, b; c; z)/\Gamma(c)$ is the regularized hypergeometric function.

The map g corresponding to $\tilde{\theta} = \pi/4$ is illustrated in figure 5*a*, and the complex constant $a(\tilde{\theta}) = a_1(\tilde{\theta}) + \imath a_2(\tilde{\theta})$, where $a_1 = \alpha\beta/(\beta^2 + \gamma^2)$ and $a_2 = \alpha\gamma/(\beta^2 + \gamma^2)$, is shown in figure 5*b*. Note that although α, β and γ are singular at $\tilde{\theta} = \pi/2$, a_1 and a_2 are not.

We now write the problem in the ζ plane. If w_1 satisfies (A 1) in D, $W_1(\zeta) := w_1(g(\zeta))$ satisfies the following problem in D':

$$\left.\begin{array}{ll} \Delta_\zeta W_1 = 0 & |\zeta| < 1, \\ \mathrm{Im}(W_1) = 0 & |\zeta| = 1 \\ W_1 \sim -a(\tilde{\theta})\zeta^{-1} & \text{at } 0, \end{array}\right\} \tag{A 4}$$

where Δ_ζ denotes the Laplacian operator in the ζ-plane. The solution to (A 4) is

$$W_1(\zeta) = -\left(\overline{a}(\tilde{\theta})\zeta + \frac{a(\tilde{\theta})}{\zeta}\right). \tag{A 5}$$

Repeating the same procedure to solve for (3.25), we find that $u_2 = \mathrm{Re}(w_2)$, where w_2 satisfies (A 1) but replacing the condition at infinity by $w_2 \sim -\imath z$. Then the solution in the ζ plane $W_2(\zeta) := w_2(g(\zeta))$ needs to go like $ia(\tilde{\theta})/\zeta$ at the origin and is therefore given by

$$W_2(\zeta) = -\imath\left(\overline{a}(\tilde{\theta})\zeta - \frac{a(\tilde{\theta})}{\zeta}\right). \tag{A 6}$$

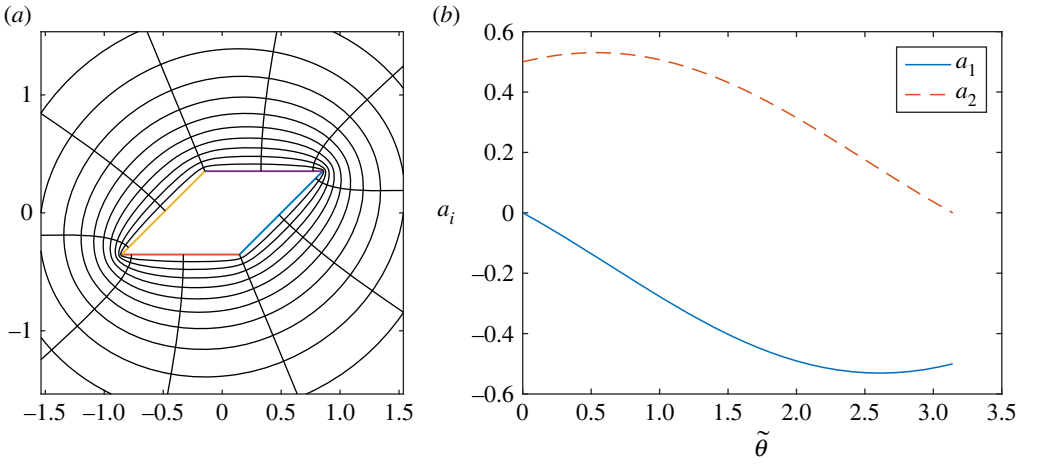

Figure 5. (*a*) Schwarz–Christoffel map g in (A 2) from the interior of unit circle to the exterior of the rhombus, for $\tilde{\theta} = \pi/4$. The black curves are the images of 10 evenly spaced circles centred at the origin and 10 evenly spaced radii in the unit disk. Plot generated using the Schwarz–Christoffel MATLAB Toolbox [41]. (*b*) Real and imaginary parts of the multiplicative constant $a(\tilde{\theta})$ (A 3).

Appendix B. Collision integral

In this appendix, we evaluate the integral J in (3.29),

$$J = \int_{\partial \mathcal{R}_{\tilde{\theta}}} R_{\theta_1}^T \nabla_{\tilde{\mathbf{x}}_1} \tilde{P}^{(1)} \cdot \tilde{\mathbf{n}} \, \mathrm{d}S_{\tilde{\mathbf{x}}}, \tag{B 1}$$

where $\mathcal{R}_{\tilde{\theta}}$ is the excluded rhombus in the inner region with $|\mathcal{R}_{\tilde{\theta}}| = \sin\tilde{\theta}$ (remark (3.1)). By using the first-order inner solution $\tilde{P}^{(1)}$ (3.23), we write $J = J_A + J_B + J_C$ with

$$\left.\begin{aligned} J_A &= \int_{\partial \mathcal{R}_{\tilde{\theta}}} R_{\theta_1}^T \nabla_{\tilde{\mathbf{x}}_1} (R_{\theta_1}^T \mathbf{A} \cdot \tilde{\mathbf{x}}) \cdot \tilde{\mathbf{n}} \, \mathrm{d}S_{\tilde{\mathbf{x}}} = \nabla_{\tilde{\mathbf{x}}_1} \cdot \left[R_{\theta_1} \left(\int_{\partial \mathcal{R}_{\tilde{\theta}}} \tilde{\mathbf{x}} \otimes \tilde{\mathbf{n}} \, \mathrm{d}S_{\tilde{\mathbf{x}}} \right) R_{\theta_1}^T \mathbf{A} \right], \\ J_B &= \int_{\partial \mathcal{R}_{\tilde{\theta}}} R_{\theta_1}^T \nabla_{\tilde{\mathbf{x}}_1} (R_{\theta_1}^T \mathbf{B} \cdot \mathbf{u}) \cdot \tilde{\mathbf{n}} \, \mathrm{d}S_{\tilde{\mathbf{x}}} = \nabla_{\tilde{\mathbf{x}}_1} \cdot \left[R_{\theta_1} \left(\int_{\partial \mathcal{R}_{\tilde{\theta}}} \mathbf{u} \otimes \tilde{\mathbf{n}} \, \mathrm{d}S_{\tilde{\mathbf{x}}} \right) R_{\theta_1}^T \mathbf{B} \right] \end{aligned}\right\} \tag{B 2}$$

and

$$J_C = R_{\theta_1}^T \nabla_{\tilde{\mathbf{x}}_1} C_\infty \cdot \int_{\partial \mathcal{R}_{\tilde{\theta}}} \tilde{\mathbf{n}} \, \mathrm{d}S_{\tilde{\mathbf{x}}}.$$

We have $J_C = 0$ since we integrate the normal along the closed curve $\partial \mathcal{R}_{\tilde{\theta}}$. To evaluate J_A and J_B, we are left to compute the matrices inside the round brackets, which we denote by $-Q$ and $-T$, respectively,

$$Q = -\int_{\partial \mathcal{R}_{\tilde{\theta}}} \tilde{\mathbf{x}} \otimes \tilde{\mathbf{n}} \, \mathrm{d}S_{\tilde{\mathbf{x}}} \quad \text{and} \quad T = -\int_{\partial \mathcal{R}_{\tilde{\theta}}} \mathbf{u} \otimes \tilde{\mathbf{n}} \, \mathrm{d}S_{\tilde{\mathbf{x}}}.$$

The first row of Q is

$$Q_{1\cdot} = -\int_{\partial \mathcal{R}_{\tilde{\theta}}} \tilde{x} \tilde{\mathbf{n}} \, \mathrm{d}S_{\tilde{\mathbf{x}}} \sim \int_{\mathcal{R}_{\tilde{\theta}}} \nabla_{\tilde{\mathbf{x}}} \tilde{x} \, \mathrm{d}\tilde{\mathbf{x}} = (1, 0) \int_{\mathcal{R}_{\tilde{\theta}}} \mathrm{d}\tilde{\mathbf{x}} = (1, 0) \sin\tilde{\theta}, \tag{B 3}$$

applying the divergence theorem (on $\tilde{x}\mathbf{c}$ with $\mathbf{c}$ constant). The $\sim$ equivalence is due to the fact that $\tilde{\mathbf{n}}$ is the projection of the unit normal $\tilde{n}$ onto the $\tilde{\mathbf{x}}$ plane, and so it is not normalized (see (3.15) and discussion thereafter). However, since the component of $\tilde{n}$ in the $\tilde{\theta}$ direction is $O(\epsilon)$, and we only require the leading order of J, we can treat $\tilde{\mathbf{n}}$ as if it were the unit normal on $\mathcal{R}_{\tilde{\theta}}$. For example, on the top edge of the rhombus, we have $\tilde{\mathbf{n}} \sim (0, -1)$ (figure 1). Note also the change in sign in the

royalsocietypublishing.org/journal/rspa Proc. R. Soc. A 479: 20230076

first equivalence since $\tilde{\mathbf{n}}$ is the inward unit normal to $\mathcal{R}_{\tilde{\theta}}$. Similarly, we find that the second row of Q is expressed as follows:

$$Q_{2\cdot} = -\int_{\partial\mathcal{R}_{\tilde{\theta}}} \tilde{y}\tilde{\mathbf{n}}\,\mathrm{d}S_{\tilde{\mathbf{x}}} \sim (0,1)\sin\tilde{\theta}. \tag{B 4}$$

Therefore, we find that $Q(\tilde{\theta}) = \sin\tilde{\theta} I_2$. Matrix T has rows

$$T_{i\cdot} = -\int_{\partial\mathcal{R}_{\tilde{\theta}}} u_i(\tilde{\mathbf{x}})\tilde{\mathbf{n}}\,\mathrm{d}S_{\tilde{\mathbf{x}}}, \tag{B 5}$$

where u_i for $i = 1, 2$ solve (3.24) and (3.25), respectively. Rather than transforming the solutions W_1 and W_2 obtained in appendix A back to the $\tilde{\mathbf{x}}$ plane, we express the integrals as complex integrals in the ζ plane (figure 4). To transform (B 5) into a complex integral, first recall that $z = \tilde{x} + \imath\tilde{y}$. Given a parameterization $(\tilde{x}(s), \tilde{y}(s))$ of $\partial\mathcal{R}_{\tilde{\theta}} \equiv \Gamma$, the integral along the arc length is

$$\mathrm{d}S_{\tilde{\mathbf{x}}} \equiv \mathrm{d}\mathbf{s} = (\tilde{x}'(s), \tilde{y}'(s))\,\mathrm{d}s = (\tilde{x}'(s) + \imath\tilde{y}'(s))\,\mathrm{d}s = z'(s)\,\mathrm{d}s = \mathrm{d}z.$$

Since the curves Γ and Γ' are positively oriented (figure 4), the corresponding outward normals to the interior of the rhombus or the exterior of the circle, respectively, are given by a $-\pi/2$ rotation, or $-\imath$, of the tangent vector. Therefore, T_i as a complex integral is

$$T_{i\cdot} = \imath\int_{\Gamma} u_i(z)\,\mathrm{d}z = \imath\int_{\Gamma} w_i(z)\,\mathrm{d}z = \imath\int_{\Gamma'} W_i(\zeta)g'(\zeta)\,\mathrm{d}\zeta. \tag{B 6}$$

In the second equality, we have used that $\mathrm{Im}(w_i) = 0$ on Γ (A 1) and in the third that $W_i(\zeta) = w_i(g(\zeta))$.

The integrand in (B 6) has a singularity at the origin and branch points at ± 1 and $\pm\imath$. We choose branch cuts going to infinity so that the contour of integration follows Γ' with four small semicircular indentations at the branch points as shown in figure 6. This way, $T_{i\cdot}$ can be computed using Cauchy's residue theorem, with $2\pi\imath$ times the residue at the origin and $-\pi\imath$ times the residues at the four branch points.[2] In fact, the four branch points do not contribute to the integral for $\tilde{\theta} \in (0, \pi)$ as their residues are zero (no singularities). Because of the form of $W_1(\zeta)$ and $W_2(\zeta)$ ((A 5) and (A 6)), it is sufficient to compute the following residues

$$\mathrm{Res}_{\zeta=0}[\zeta g'(\zeta)] = a(\tilde{\theta}) \quad \text{and} \quad \mathrm{Res}_{\zeta=0}[\zeta^{-1}g'(\zeta)] = \left(1 - \frac{2\tilde{\theta}}{\pi}\right)a(\tilde{\theta}). \tag{B 7}$$

By substituting in the expressions for W_i (A 5) and (A 6) in (B 6) and using (B 7), we find

$$\begin{aligned} T_{1\cdot} &= -\imath\int_{\Gamma'}\left(\bar{a}(\tilde{\theta})\zeta + \frac{a(\tilde{\theta})}{\zeta}\right)g'(\zeta)\,\mathrm{d}\zeta = 2\pi\{\bar{a}\,\mathrm{Res}_{\zeta=0}[\zeta g'(\zeta)] + a\,\mathrm{Res}_{\zeta=0}[\zeta^{-1}g'(\zeta)]\} \\ &= 2\pi a\bar{a} - (4\tilde{\theta} - 2\pi)\,a^2, \end{aligned} \tag{B 8}$$

and

$$\begin{aligned} T_{2\cdot} &= \int_{\Gamma'}\left(\bar{a}(\tilde{\theta})\zeta - \frac{a(\tilde{\theta})}{\zeta}\right)g'(\zeta)\,\mathrm{d}\zeta = 2\pi\imath\{\bar{a}\,\mathrm{Res}_{\zeta=0}[\zeta g'(\zeta)] - a\,\mathrm{Res}_{\zeta=0}[\zeta^{-1}g'(\zeta)]\} \\ &= 2\pi\imath a\bar{a} + \imath(4\tilde{\theta} - 2\pi)a^2. \end{aligned} \tag{B 9}$$

By writing (B 8) and (B 9) as two-dimensional vectors, we obtain the symmetric matrix

$$T(\tilde{\theta}) := -\int_{\partial\mathcal{R}_{\tilde{\theta}}} \mathbf{u}\otimes\tilde{\mathbf{n}}\,\mathrm{d}S_{\tilde{\mathbf{x}}} = 4\begin{bmatrix} a_1^2(\pi - \tilde{\theta}) + a_2^2\tilde{\theta} & a_1a_2(\pi - 2\tilde{\theta}) \\ a_1a_2(\pi - 2\tilde{\theta}) & a_2^2(\pi - \tilde{\theta}) + a_1^2\tilde{\theta} \end{bmatrix}, \tag{B 10}$$

where a_1 and a_2 are shown in figure 5*b*.

[2]Note that the contribution of the four points on the unit circle is $-\pi\imath$ since it is only half a circle, and we are taking the small semicircles clockwise.

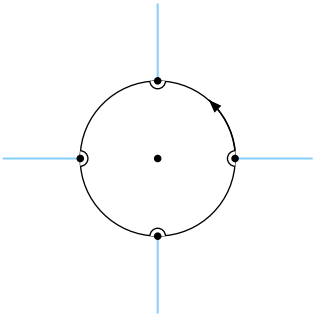

Figure 6. Contour to compute the integral (B 6).

References

1. D'Orsogna MR, Chuang Y, Bertozzi AL, Chayes LS. 2006 Self-propelled particles with soft-core interactions: patterns, stability, and collapse. *Phys. Rev. Lett.* **96**, 104302. (doi:10.1103/PhysRevLett.96.104302)
2. Bruna M, Chapman SJ. 2012 Excluded-volume effects in the diffusion of hard spheres. *Phys. Rev. E* **85**, 011103. (doi:10.1103/PhysRevE.85.011103)
3. Snodin BE *et al.* 2015 Introducing improved structural properties and salt dependence into a coarse-grained model of DNA. *J. Chem Phys.* **142**, 06B613_1. (doi:10.1063/1.4921957)
4. Bahadur B. 1990 *Liquid crystals: applications and uses*, vol. 1. Singapore: World Scientific.
5. Cates ME, Tailleur J. 2015 Motility-induced phase separation. *Annu. Rev. Condens. Matter Phys.* **6**, 219–244. (doi:10.1146/annurev-conmatphys-031214-014710)
6. Carrillo JA, Fornasier M, Toscani G, Vecil F. 2010 Particle, kinetic, and hydrodynamic models of swarming, In *Mathematical modeling of collective behavior in socio-economic and life sciences* (eds G Naldi, L Pareschi, G Toscani), pp. 297–336. Boston, MA: Birkhäuser.
7. Cucker F, Smale S. 2007 Emergent behavior in flocks. *IEEE Trans. Automat. Contr.* **52**, 852–862. (doi:10.1109/TAC.2007.895842)
8. Vicsek T, Czirók A, Ben-Jacob E, Cohen I, Shochet O. 1995 Novel type of phase transition in a system of self-driven particles. *Phys. Rev. Lett.* **75**, 1226–1229. (doi:10.1103/PhysRevLett.75.1226)
9. Degond P, Manhart A, Yu H. 2017 A continuum model for nematic alignment of self-propelled particles. *Discrete Contin. Dyn. Syst.-B* **22**, 1295–1327. (doi:10.3934/dcdsb.2017063)
10. Jabin PE, Wang Z. 2017 Mean field limit for stochastic particle systems. In *Active particles*, vol. 1 (eds N Bellomo, P Degond, E Tadmor), pp. 379–402. Cham, Switzerland: Birkhäuser.
11. Topaz CM, Bertozzi AL, Lewis MA. 2006 A nonlocal continuum model for biological aggregation. *Bull. Math. Biol.* **68**, 1601–1623. (doi:10.1007/s11538-006-9088-6)
12. Hoffmann FKO. 2017 *Keller-Segel-type models and kinetic equations for interacting particles: long-time asymptotic analysis*. PhD thesis, University of Cambridge, Cambridge, UK.
13. Carrillo JA, D'Orsogna MR, Panferov V. 2009 Double milling in self-propelled swarms from kinetic theory. *Kinet. Relat. Models* **2**, 363. (doi:10.3934/krm.2009.2.363)
14. Hittmeir S, Kanzler L, Manhart A, Schmeiser C. 2021 Kinetic modelling of colonies of myxobacteria. *Kinet. Relat. Models* **14**, 1–24. (doi:10.3934/krm.2020046)
15. Kanzler L, Schmeiser C. 2023 Kinetic model for myxobacteria with directional diffusion. *Commun. Math. Sci.* **21**, 107–126. (doi:10.4310/CMS.2023.v21.n1.a5)
16. Gay J, Berne B. 1981 Modification of the overlap potential to mimic a linear site–site potential. *J. Chem. Phys.* **74**, 3316–3319. (doi:10.1063/1.441483)
17. Berne BJ, Pechukas P. 1972 Gaussian model potentials for molecular interactions. *J. Chem. Phys.* **56**, 4213–4216. (doi:10.1063/1.1677837)
18. Marth W, Praetorius S, Voigt A. 2015 A mechanism for cell motility by active polar gels. *J. R. Soc. Interface* **12**, 20150161. (doi:10.1098/rsif.2015.0161)
19. Wenzel D, Voigt A. 2021 Multiphase field models for collective cell migration. *Phys. Rev. E* **104**, 054410. (doi:10.1103/PhysRevE.104.054410)

20. Onsager L. 1949 The effects of shape on the interaction of colloidal particles. *Ann. N.Y. Acad. Sci.* **51**, 627–659. (doi:10.1111/j.1749-6632.1949.tb27296.x)
21. Farrell FDC, Marchetti MC, Marenduzzo D, Tailleur J. 2012 Pattern formation in self-propelled particles with density-dependent motility. *Phys. Rev. Lett.* **108**, 248101. (doi:10.1103/PhysRevLett.108.248101)
22. Doumic M, Hecht S, Peurichard D. 2020 A purely mechanical model with asymmetric features for early morphogenesis of rod-shaped bacteria micro-colony. *Math. Biosci. and Eng.* **17**, 6873–6908. (doi:10.3934/mbe.2020356)
23. Holcman D, Schuss Z. 2012 Brownian needle in dire straits: Stochastic motion of a rod in very confined narrow domains. *Phys. Rev. E* **85**, 010103. (doi:10.1103/PhysRevE.85.010103)
24. Chen H, Thiffeault JL. 2021 Shape matters: a Brownian microswimmer in a channel. *J. Fluid Mech.* **916**, A15. (doi:10.1017/jfm.2021.144)
25. Doi M, Edwards SF. 1986 *The theory of polymer dynamics*. International series of monographs on physics, vol. 73. Oxford: Clarendon Press.
26. De Gennes PG, Prost J. 1993 *The physics of liquid crystals*. Oxford Science Publications, vol. 83, 2nd edn. Oxford: Clarendon Press.
27. Frenkel D, Maguire JF. 1981 Molecular dynamics study of infinitely thin hard rods: scaling behavior of transport properties. *Phys. Rev. Lett.* **47**, 1025–1028. (doi:10.1103/PhysRevLett.47.1025)
28. Mandal S, Kurzthaler C, Franosch T, Löwen H. 2020 Crowding-enhanced diffusion: an exact theory for highly entangled self-propelled stiff filaments. *Phys. Rev. Lett.* **125**, 138002. (doi:10.1103/PhysRevLett.125.138002)
29. Bruna M, Chapman SJ. 2012 Diffusion of multiple species with excluded-volume effects. *J Chem. Phys.* **137**, 204116. (doi:10.1063/1.4767058)
30. Kayser RF, Raveché HJ. 1978 Bifurcation in Onsager's model of the isotropic-nematic transition. *Phys. Rev. A* **17**, 2067–2072. (doi:10.1103/PhysRevA.17.2067)
31. Gardiner CW. 2009 *Stochastic methods: a handbook for the natural and social sciences*. Berlin: Springer.
32. Bruna M, Burger M, Esposito A, Schulz S. 2022 Phase separation in systems of interacting active brownian particles. *SIAM J. Appl. Math.* **82**, 1635–1660. (doi:10.1137/21M1452524)
33. Leitmann S, Höfling F, Franosch T. 2017 Dynamically crowded solutions of infinitely thin Brownian needles. *Phys. Rev. E* **96**, 012118. (doi:10.1103/PhysRevE.96.012118)
34. Carrillo J, Gvalani R, Pavliotis G, Schlichting A. 2020 Long-time behaviour and phase transitions for the McKean–Vlasov equation on the torus. *Arch. Ration. Mech. Anal.* **235**, 635–690. (doi:10.1007/s00205-019-01430-4)
35. Kuramoto Y. 1981 Rhythms and turbulence in populations of chemical oscillators. *Phys. A: Stat. Mech. Appl.* **106**, 128–143. (doi:10.1016/0378-4371(81)90214-4)
36. Frenkel D, Eppenga R. 1985 Evidence for algebraic orientational order in a two-dimensional hard-core nematic. *Phys. Rev. A* **31**, 1776. (doi:10.1103/PhysRevA.31.1776)
37. Driscoll TA, Hale N, Trefethen LN. 2014 *Chebfun guide*. Oxford, UK: Pafnuty Publications.
38. Mason J, Jack RL, Bruna M. 2023 Macroscopic behaviour in a two-species exclusion process via the method of matched asymptotics. *J. Stat. Phys.* **190**, 47. (doi:10.1007/s10955-022-03036-9)
39. Bruna M, Chapman SJ, Schmidtchen M. 2023 Derivation of a macroscopic model for Brownian hard needles. Figshare. (doi:10.6084/m9.figshare.c.6673715)
40. Driscoll TA, Trefethen LN. 2002 *Schwarz–Christoffel mapping*. Cambridge monographs on applied and computational mathematics, vol. 8. Cambridge University Press, Cambridge, UK.
41. Driscoll TA. 2003 Schwarz–Christoffel Toolbox for MATLAB. Version 2.3.